Numerical Shape Optimization of Airfoils With Practical Aerodynamic Design Requirements

by

Jens Howard Peter Buckley

A thesis submitted in conformity with the requirements
for the degree of Masters of Applied Science
Graduate Department of Aerospace Engineering
University of Toronto

Abstract

Numerical Shape Optimization of Airfoils With Practical Aerodynamic Design Requirements

Jens Howard Peter Buckley

Masters of Applied Science

Graduate Department of Aerospace Engineering

University of Toronto

2009

Practical aerodynamic shape design problems must balance the goal of performance optimization over a range of on-design operating conditions with the need to meet design constraints at various off-design operating conditions. Such design problems can be cast as multipoint optimization problems where the on-design and off-design operating conditions are represented as design points with corresponding objective or constraint functions. Two methods are presented for obtaining optimal airfoil designs that satisfy all design objectives and constraints. The first method uses an unconstrained optimization algorithm where the optimal design is achieved by minimizing a weighted sum of the objective functions at each of the operating conditions. To address the competing design objectives between on-design and off-design operating conditions, an automated procedure is used to weight the off-design objective functions so as to limit their influence on the overall optimization, while satisfying the design constraints. The second method uses the constrained optimization algorithm SNOPT, which allows the aerodynamic constraints imposed at the off-design operating conditions to be treated explicitly. Both methods are applied to the design of an airfoil for a hypothetical aircraft, which is formulated as an 18-point multipoint optimization.

Acknowledgements

I would like to thank David Zingg for providing the perfect balance of guidance and flexibility that made it possible for me to pursue this work. That he is a gifted teacher with a vast wealth of knowledge and wisdom goes without saying. His encouragement and confidence in my abilities compelled me to produce my best work.

Thanks to Beckett Zhou for many helpful discussions regarding the inner workings of Optima2D and the underlying concepts of the methods described herein.

I am lucky to have parents who have always been supportive of my endeavours and shown an interest in my work. They have also been excellent role models to me and piqued my interest in a scientific career.

To my wife Shirley and my daughter Madeleine, thank you for providing an escape from my school-related thoughts. You have kept me energized and inspired during this exciting time. Thank you for serving as a constant reminder of what is truly important in life.

Financial support from The University of Toronto, Bombardier, Canada Research Chairs, MITACS, and the Natural Sciences and Engineering Research Council of Canada is gratefully acknowledged.

Contents

Chapter 1

Introduction

The aircraft design process applied in industry is a complex endeavour that involves concurrent engineering of the many systems that comprise a fully functional aircraft. In addition to the aerodynamic performance of an aircraft, equal consideration must be given to the disciplines tasked with specifying appropriate structures, controls, materials, and propulsion systems necessary to satisfy a truly comprehensive set of design requirements. In this day and age, where greenhouse gas emissions associated with commercial aviation are of public concern with regard to climate change, and rising jet fuel prices are negatively impacting profits of commercial carriers, the design objective of improving aircraft fuel efficiency has become increasingly important. If it can be shown that a novel aerodynamic shape will provide the greatest improvement in aircraft fuel efficiency, then this shape should drive the design process such that the above mentioned disciplines strive to adapt their systems in order to minimize divergence from this optimal shape.

The coupling of computational fluid dynamics with numerical optimization techniques has resulted in aerodynamic shape optimization algorithms that are efficient at producing aircraft shape configurations with improved performance characteristics at a given aircraft operating condition. While significant progress in the field of aerodynamic shape optimization has been made over the past 20 years, further advancement is still required

to make numerical optimization techniques useful to solve practical aerodynamic design problems. Practical aerodynamic design problems are characterized by comprehensive design requirements that must be satisfied over a broad range of aircraft operating conditions. For aerodynamic shape optimization to be considered a viable alternative to the traditional *cut-and-try* approach to aerodynamic design, it must be capable of producing an optimal design that satisfies the design requirements over this broad range of operating conditions. This type of optimization, in which more than one aircraft operating condition is considered, is commonly referred to as multipoint optimization.

1.1 Overview of Aerodynamic Shape Optimization

In general, the goal of an aerodynamic design process is to find an aerodynamic shape that achieves a given set of design objectives. Within the context of aircraft design, the aerodynamic design process is applied to the shape of various components of the aircraft that interact with the surrounding air to provide lift, stability, and control. The wings of an aircraft are obvious examples of aerodynamic shapes that are subject to the design process. A common design objective is to minimize drag on the wings while generating adequate lift required to keep the aircraft aloft. An optimal aerodynamic design is one that best satisfies the design objectives. Referring to the above design objective example, there may be many wing configurations that satisfy the lift requirements, but only the *optimal solution* satisfies the lift requirements *and* has the lowest drag of all the configurations under consideration.

Aerodynamic shape optimization can be used as a design tool to produce optimal configurations with respect to design objectives. Design objectives and operating conditions are translated into optimization problems that can be solved by numerical methods. The following provides a brief overview of the aerodynamic optimization process. A flow solver is used to determine the properties of the flow field around an aerodynamic shape

at a given set of operating conditions. The flow solution yields the properties of the flow field that are used to determine performance characteristics of the shape such as lift and drag. An objective function is formulated to evaluate the performance of the shape with respect to the design objectives. A mathematical representation of the geometry of the shape provides a means to make alterations to the shape via design variables. An optimization algorithm uses information about the objective function at the current design iteration to determine how to modify the design variables to improve the performance of the shape. The updated shape specified by the modified design variables is presented to the flow solver and the process is repeated iteratively until criteria are satisfied indicating that an optimal solution has been achieved and no further improvement in performance is possible.

The simplest aerodynamic optimization problem is to find a shape with the best performance at a single operating condition. For example, to find the shape of a wing that has the minimum drag when flying at an expected cruising speed for the aircraft. This type of optimization problem is referred to as a single-point optimization. The drawback of a single point optimization in some cases is that performance degrades significantly with even the slightest deviation from the expected operating condition.

A multi-objective optimization problem seeks to find a shape where the optimal performance is a compromise between competing design objectives at a common operating condition. For example, it may be desireable to have a wing that generates a high lift coefficient at a given operating condition and we may also want to minimize the drag on the wing at this operating condition. However, increased lift comes at the expense of increased drag, and conversely, a reduction in drag is achieved by sacrificing lift. One option is to perform a single-point optimization with the objective function formulated to maximize the lift to drag ratio. Alternatively, each of the design objectives can be represented with separate objective functions. Each objective function is specified as part of a design point definition along with an operating condition that is common to

both design points. A composite objective function may be formed as a weighted sum of the individual objective functions at their respective design points. Multi-objective optimization has the benefit of allowing the competing design objectives to be prioritised via weight assignments.

Regarding multi-objective optimization problems, a designer may be interested in the trade-offs in performance associated with each of the design objectives. A Pareto front defines a family of optimal solutions to a multi-objective optimization problem obtained by varying the weights associated with each of the design objectives. By plotting the competing performance values for the set of Pareto-optimal solutions, a designer can quickly visualize these trade-offs and select the design that achieves the most appropriate compromise.

The extension of the concept of multi-objective optimization leads to a more generalized problem formulation where multiple design points are considered, each potentially having a unique objective function and operating condition. This is commonly referred to as multipoint optimization. As with multi-objective optimization, a composite objective function is formed as a weighted sum of the objective functions at each design point. The highly localized solutions typical of single-point optimization can be de-sensitized to variations in operating conditions by performing a multipoint optimization over a range of operating conditions.

1.2 Review of Multipoint Optimization Applications

Researchers have addressed the topic of multipoint optimization under various contexts within the realm of aerodynamic design problems. Recently, Epstein et al. [5] used multipoint optimization to minimize wing drag at the main cruise operating condition and nearby secondary cruise operating conditions. Cliff et al. [3] compare two approaches to multipoint optimization as applied to the aerodynamic shape optimization of the NASA

Technology Concept Airplane, simultaneous multipoint design vs. sequential cruise-point design followed by trim optimization at transonic conditions. Zingg and Elias [26] as well as Li et al. [8] have used multipoint optimization techniques applied to airfoil design to achieve constant drag over a range of cruise Mach numbers. Although significant contributions have been made by these researchers and others in the area of multipoint optimization, the scope of its application to practical aerodynamic design problems has been limited.

1.3 Practical Aerodynamic Design Problems

The design requirements of a practical aerodynamic design problem must consider the broad range of operating conditions that an aircraft is expected to encounter within its flight envelope. These design requirements correspond to the intended flight mission of the aircraft. An aircraft intended for regional flights may spend most of its time ascending and descending to and from cruise speed and altitude and a relatively short time flying at these cruise conditions, whereas an aircraft intended for trans-continental flights will spend the majority of its time at cruise conditions. Lift requirements also vary significantly over the duration of a flight due to changes in weight as fuel is consumed. In any case there are several distinct areas within the flight envelope having widely varying operating conditions and design requirements. An aircraft must operate efficiently over this range of flight Mach numbers and lift requirements.

A dichotomy exists in practical aerodynamic design problems between optimizing performance and satisfying design constraints. Constraints are required to ensure that the design is feasible with respect to manufacturing capabilities, structural soundness, safety requirements, etc. The distinction between performance goals and constraints can be addressed within a multipoint optimization framework by designating design points as either on-design or off-design. In a multipoint optimization problem formulation, *on-*

design points refer to the operating conditions where it is desired to optimize aerodynamic performance according to specified design objectives. For example, we may wish to optimize an aerodynamic shape such that drag is minimized over a range of expected cruise Mach numbers and lift requirements. Whereas *off-design* points refer to operating conditions where aerodynamic constraints are imposed on the optimization. For example, the off-design requirement that an aerodynamic shape must have high lift at low speeds constrains the potential for drag minimization at cruise conditions.

The work described in this thesis follows from the investigation of multipoint optimization applied to practical aerodynamic design problems undertaken by Zingg and Billing [25]. Their goal was to demonstrate that multipoint optimization techniques can be applied to complex aerodynamic design problems that encompass a broad range of requirements extending beyond typical *drag-minimization-over-a-range-of-cruise-conditions* objectives. This broad range of design requirements also includes high lift at low speed and consideration of maneuverability under dive conditions. Zingg and Billing used a design specification for a hypothetical aircraft as the basis for a practical aerodynamic design problem. The design specification was used to define a multipoint optimization problem consisting of 18 design points categorized as either on-design points or off-design points. The optimization algorithm used by Zingg and Billing minimized a weighted sum of the objective functions at each of the design points given by:

$$J_{comp} = \sum_{i=1}^{18} \omega_i J_i \tag{1.1}$$

where ω_i and J_i are the weights and objective functions, respectively, at the design points. The methods presented herein for solving practical aerodynamic design problems focus on several key findings from their investigation:

1. Performance at on-design operating conditions is compromised by the need to satisfy off-design constraints.

2. On-design performance may be unnecessarily sacrificed if off-design constraints are over-satisfied.

3. Over-satisfaction of off-design constraints may be prevented by appropriate selection of their respective off-design weights.

The off-design weights mentioned above refer to the weights applied to the respective off-design objective functions in the composite objective function. A problem with multipoint optimization noted by several researchers [26, 8] is that the appropriate off-design weights are not known a priori. As implied by the findings of Zingg and Billing, a poor assignment of off-design weights will result in one of two outcomes:

1. The off-design constraints are violated, or

2. The on-design performance is unnecessarily compromised

One might assume that there is an ideal weight value for any given off-design point that will result in a final optimized shape where its constraint value is exactly satisfied. However, a practical aerodynamic design problem may include off-design points that will have their constraints satisfied regardless of the weight applied to them, referred to as *redundant* points. Given this property of redundant off-design points, their ideal weight is zero.

1.4 Objectives

The work presented in this thesis investigates the application of two different methods to solve a practical aerodynamic design problem. The goal of the first method using an unconstrained optimization algorithm is to determine the ideal weights for all of the off-design points considered in a practical aerodynamic design problem in a way that *does not require user intervention*. A procedure is introduced for automatically obtaining the

ideal off-design weights by exploiting aerodynamic performance trends as they evolve throughout the optimization. The second method uses the constrained optimization algorithm SNOPT, which allows the aerodynamic constraints imposed at the off-design operating conditions to be treated explicitly. The off-design points in this method are not included in the composite objective function (which contains only on-design objectives). Rather they are used as constraints in conjunction with the composite objective function to define a Lagrangian function that we seek to minimize to find the optimal solution.

The main objective of this work is to characterize, evaluate, and compare these two different approaches to solving practical aerodynamic design problems. When assessing the merits of these methods, foremost consideration is given to their ability to optimize performance at on-design operating conditions while ensuring that design constraints at off-design operating conditions are satisfied. Further consideration is given to the level of user expertise and involvement required to achieve an optimal solution to the design problem. In this respect, a method that requires minimal user intervention is highly desireable, and accordingly, the development of a method that is fully automated is a top priority. Finally, the computational effort required to solve a practical aerodynamic design problem is a significant factor in the viability of any method. With regards to both methods, steps are taken to improve overall computational efficiency.

Chapter 2

The Optima2D Platform

Generally speaking, to solve an aerodynamic shape optimization problem, an optimization algorithm is required to determine how to modify the design variables, X, to optimize performance according to the design objectives. Working in conjunction with the optimization algorithm, a set of tools is required to evaluate candidate designs obtained from modified design variables during the course of an optimization.

The two methods for solving practical aerodynamic design problems described in this thesis both make use of a common set of design evaluation tools contained within the two-dimensional airfoil optimization algorithm Optima2D. A summarized description of these tools is provided in the following sections.

2.1 Airfoil Geometry Manipulation Using B-Spline Curves

Cubic B-spline curves are used to represent a wide range of airfoil shapes during the course of an optimization. The parametric representation of an airfoil shape with a

B-spline curve is given by

$$x_a(w_j) = \sum_{i=1}^{n+1} X_i^c B_{i,k}(w_j) \tag{2.1}$$

$$y_a(w_j) = \sum_{i=1}^{n+1} Y_i^c B_{i,k}(w_j) \tag{2.2}$$

where (x_a, y_a) are the Cartesian coordinates of the airfoil surface, $B_{i,k}$ are the B-spline basis functions, (X_i^c, Y_i^c) are the coordinates of the B-spline control points, and $n+1$ is the total number of control points. The optimization algorithm modifies the vertical coordinates, Y_i^c, of the B-spline control points to make local changes to the airfoil geometry. These parameters are referred to as geometric design variables.

2.2 Grid Perturbation

After the airfoil geometry has been modified by manipulation of the geometric design variables, the computational grid surrounding the airfoil must conform to the changes in geometry in such a way that the accuracy of the flow solution is preserved. An algebraic grid perturbation strategy is used to perform this task and is given by

$$y_k^{\text{new}} = y_k^{\text{old}} + \frac{\Delta y}{2}\left[1 + \cos(\pi S_k)\right], \quad k = 1, \ldots, k_{\max} - 1 \tag{2.3}$$

where Δy represents the airfoil shape change. S_k is the normalized arclength distance given by

$$S_1 = 0$$

$$S_k = \frac{1}{L_g}\sum_{i=2}^{k} L_i, \quad k = 2, \ldots, k_{\max} - 1 \tag{2.4}$$

where L_i is the length of a segment between nodes k and $k-1$. L_g is the grid-line length from the body to the outer boundary given by

$$L_g = \sum_{i=2}^{k_{\max}} L_i \tag{2.5}$$

2.3 Flow Solver

At each design iteration, the flow around the airfoil represented by the compressible Reynolds-averaged Navier-Stokes equations is solved with the Newton-Krylov method developed by Nemec and Zingg [11, 12]. A brief description of the main features of this flow solver are provide in this section.

For a two-dimensional flow in Cartesian coordinates (x, y) with density ρ, velocities (u, v), and total energy e, the compressible Navier-Stokes equations are given by

$$\frac{\partial Q}{\partial t} + \frac{\partial E}{\partial x} + \frac{\partial F}{\partial y} = \mathcal{R}e^{-1}\left(\frac{\partial E_v}{\partial x} + \frac{\partial F_v}{\partial y}\right) \tag{2.6}$$

where Q is the vector of conservative flow variables mass, momentum, and energy given by

$$Q = \begin{bmatrix} \rho \\ \rho u \\ \rho v \\ e \end{bmatrix} \tag{2.7}$$

The convective flux vectors are given by

$$E = \begin{bmatrix} \rho u \\ \rho u^2 + p \\ \rho uv \\ u\,(e+p) \end{bmatrix} \quad \text{and} \quad F = \begin{bmatrix} \rho u \\ \rho uv \\ \rho v^2 + p \\ v\,(e+p) \end{bmatrix} \tag{2.8}$$

and the viscous flux vectors are given by

$$E_v = \begin{bmatrix} 0 \\ \tau_{xx} \\ \tau_{xy} \\ \varphi_1 \end{bmatrix} \quad \text{and} \quad F_v = \begin{bmatrix} 0 \\ \tau_{xy} \\ \tau_{yy} \\ \varphi_2 \end{bmatrix} \tag{2.9}$$

where $\tau_{xx}, \tau_{xy}, \tau_{yy}$ are the viscous stresses, and φ_1, φ_2 are terms associated with heat conduction. The viscous stresses include the dynamic eddy viscosity, μ_t, to account

for the effects of turbulence. The value of μ_t is determined using the Spalart-Allmaras one-equation turbulence model [19]. Pressure, p, is dependent on the flow variables and satisfies

$$p = (\gamma - 1)\left[e - \frac{1}{2}\rho\left(u^2 + v^2\right)\right] \tag{2.10}$$

from the ideal gas law, where γ is the ratio of specific heats, c_p/c_v. The sound speed, a, is given by

$$a = \sqrt{\frac{\gamma p}{\rho}} \tag{2.11}$$

To simplify the Navier-Stokes equations, the thin-layer approximation, which neglects the viscous stream-wise derivatives, is used. A coordinate transformation is used to map the curvilinear grid surrounding the airfoil in the physical domain to a grid in the computational domain having uniform spacing equal to one. Taking into account the thin-layer approximation and the coordinate transformation, the Navier-Stokes equations are re-written as

$$\frac{\partial \widehat{Q}}{\partial \tau} + \frac{\partial \widehat{E}}{\partial \xi} + \frac{\partial \widehat{F}}{\partial \eta} = \mathcal{R}e^{-1}\left(\frac{\partial \widehat{S}}{\partial \eta}\right) \tag{2.12}$$

See Pulliam and Zingg [17] for details on the thin-layer approximation and the coordinate transformation. The spatial derivatives of the Navier-Stokes equations are discretized using second-order centered differences, and the temporal derivative is neglected for steady flows, resulting in the non-linear system of equations commonly referred to as the residual, given by

$$R(\widehat{Q}, X) = \delta_\xi \widehat{E} + \delta_\eta \widehat{F} - \frac{1}{\mathcal{R}e}\delta_\eta \widehat{S} - \nabla_\xi D_\xi - \nabla_\eta D_\eta = 0 \tag{2.13}$$

The artificial dissipation terms, $\nabla_\xi D_\xi$ and $\nabla_\eta D_\eta$ are added to counteract numerical instability in the solution caused by interaction of high-frequency waves.

An inexact-Newton method is used to find the solution $\widehat{Q}$ that satisfies equation 2.13 as follows

$$\mathcal{A}^{(n)} \Delta \widehat{Q}^{(n)} = -R^{(n)} \tag{2.14}$$

where

$$\mathcal{A} = \frac{\partial R}{\partial \widehat{Q}} \tag{2.15}$$

is the flow Jacobian matrix. The linear system arising at each Newton iteration is solved inexactly using the generalized minimal residual (GMRES) Krylov subspace method to yield $\Delta\widehat{Q}^{(n)}$. The Newton update is then calculated as

$$\widehat{Q}^{(n+1)} = \widehat{Q}^{(n)} + \Delta\widehat{Q}^{(n)} \tag{2.16}$$

To ensure global convergence of the Newton method, an implicit Euler time-marching scheme using the approximate-factorization approach of ARC2D in diagonal form [17] is used as a startup algorithm to obtain a good initial solution, $\widehat{Q}^{(0)}$, for equation 2.14.

2.4 Objective Functions

The flow solution, $\widehat{Q}$, is used to calculate quantifiable performance characteristics of the airfoil that are relevant to the design objectives. Two basic performance characteristics that are used in the formulation of objective functions are the coefficients of lift and drag, C_l and C_d

For the practical aerodynamic design problem considered, the on-design performance goal is to minimize drag over a range of expected cruise operating conditions. At each cruise operating condition, a specified lift coefficient must be maintained. Therefore, a lift-constrained drag minimization objective function is required and is defined as

$$\mathcal{J} = \frac{C_d}{\mathcal{J}_0} \tag{2.17}$$

where $\mathcal{J}_0 = C_{d,0}$, and $C_{d,0}$ is the drag evaluated using the initial airfoil geometry. In a multipoint optimization, all objective functions are normalized by their initial values to ensure they all start with a consistent order of magnitude. The lift constraint is satisfied using the approach described by Billing [2] whereby the angle of attack is varied within the flow solution to achieve the desired lift.

A lift maximization objective function that is used at off-design points representing high-lift requirements is of the following form

$$\mathcal{J} = \left(\frac{1}{\mathcal{J}_0}\right)\left(1 - \frac{C_l}{C_l^*}\right)^2 \tag{2.18}$$

where C_l^* represents an unattainable lift target.

2.5 Gradient Evaluation

The two approaches examined for solving practical aerodynamic design problems both use gradient-based optimization algorithms. This class of optimization algorithms makes use of the objective function and its gradient with respect to the design variables at the current design iteration to determine how to modify the design variables in order to minimize the objective function. The discrete adjoint method is used to calculate objective function gradients because the computational effort required is of the same order as a single flow solution and is almost independent of the number of design variables. Pironneau [15] was the first to recognize the benefit of the adjoint method in its application to aerodynamic shape optimization problems. The following is a brief summary of the discrete adjoint method.

Consider an objective function

$$\mathcal{J} = \mathcal{J}(\widehat{Q}, X) \tag{2.19}$$

Recall that the conservative flow variables $\widehat{Q}$ obtained from a converged flow solution must satisfy the residual of the discretized governing flow equations such that

$$R(\widehat{Q}, X) = 0 \tag{2.20}$$

A small perturbation δX of the design variables X will produce a corresponding perturbation in the objective function, $\delta\mathcal{J}$, given by

$$\delta\mathcal{J} = \frac{\partial\mathcal{J}}{\partial\widehat{Q}}\delta\widehat{Q} + \frac{\partial\mathcal{J}}{\partial X}\delta X \tag{2.21}$$

where $\delta\widehat{Q}$ can be evaluated as

$$\delta\widehat{Q} = \widehat{Q}\left(X + \delta X\right) - \widehat{Q}\left(X\right) \tag{2.22}$$

Similarly, the perturbation in the residual, δR, is given by

$$\delta\mathcal{R} = \frac{\partial R}{\partial \widehat{Q}}\delta\widehat{Q} + \frac{\partial R}{\partial X}\delta X \tag{2.23}$$

Taking into account equation 2.20, $\delta\mathcal{R} = 0$. Hence we can multiply both sides of equation 2.23 by an arbitrary vector Ψ^T and subtract from equation 2.21 to give

$$\delta\mathcal{J} = \frac{\partial \mathcal{J}}{\partial \widehat{Q}}\delta\widehat{Q} + \frac{\partial \mathcal{J}}{\partial X}\delta X - \Psi^T\left(\frac{\partial R}{\partial \widehat{Q}}\delta\widehat{Q} + \frac{\partial R}{\partial X}\delta X\right) \tag{2.24}$$

which can be rearranged as

$$\delta\mathcal{J} = \left(\frac{\partial \mathcal{J}}{\partial \widehat{Q}} - \Psi^T\frac{\partial R}{\partial \widehat{Q}}\right)\delta\widehat{Q} + \left(\frac{\partial \mathcal{J}}{\partial X} - \Psi^T\frac{\partial R}{\partial X}\right)\delta X \tag{2.25}$$

This implies that we can evaluate $\delta\mathcal{J}$ without evaluating $\delta\widehat{Q}$ (which would require an additional flow solution for each design variable) if

$$\frac{\partial \mathcal{J}}{\partial \widehat{Q}} = \Psi^T\frac{\partial \mathcal{R}}{\partial \widehat{Q}} \tag{2.26}$$

Equation 2.26 is known as the adjoint equation. It is a linear system which is solved using GMRES to obtain the adjoint solution Ψ^T. Substituting Ψ^T into equation 2.25 and rearranging reveals the gradient of the objective function with respect to the design variables

$$\mathcal{G} = \frac{\mathrm{d}\mathcal{J}}{\mathrm{d}X} = \left(\frac{\partial \mathcal{J}}{\partial X} - \Psi^T\frac{\partial \mathcal{R}}{\partial X}\right) \tag{2.27}$$

Chapter 3

Optimization Algorithms

Given the capabilities for design evaluation described in Chapter 2, an optimization algorithm is utilized to determine the values of the design variables, X, that minimize the objective function $\mathcal{J}$. The optimization problem is written mathematically as

$$\min_X \ \mathcal{J}(\widehat{Q}, X) \tag{3.1}$$

subject to constraint equations C_j

$$C_j(\widehat{Q}, X) \leq 0 \qquad j = 1, \ldots, N_c \tag{3.2}$$

where $\widehat{Q}$ is the vector of conservative flow variables, and N_c is the number of constraints.

The two methods developed to solve practical aerodynamic design problems each use a different type of optimization algorithm. Optima2D was originally developed with a quasi-Newton BFGS optimization algorithm for unconstrained optimization whose origins can be traced to the CONMIN algorithm written by Shanno and Phua [18]. The SNOPT algorithm for constrained optimization problems written by Gill, Murray, and Saunders [6] has been integrated into Optima2D as an alternative to the BFGS optimizer. The following sections provide an overview of each optimization algorithm employed.

3.1 Newton's Method for Function Minimization

Newton's method is the basis of the strategy employed by the BFGS algorithm for finding the minimum value of the function $\mathcal{J}$. For the purpose of illustration, let $\mathcal{J}$ be a scalar valued function of a single design variable x. A local minimum of $\mathcal{J}$ is found at a location x^* where its slope, defined by its first derivative, is zero and its curvature, defined by its second derivative, is positive. These are the first and second-order necessary conditions [13], respectively, for x^* to be a local minimizer of $\mathcal{J}$. The first-order necessary condition is given by

$$\mathcal{G}(x^*) = \nabla \mathcal{J}(x^*) = 0 \tag{3.3}$$

Using Newton's method to find a solution x^* that satisfies equation 3.3 gives

$$H_n \Delta x_n = -\mathcal{G}_n \tag{3.4}$$

where

$$H_n = \nabla^2 \mathcal{J}(x_n) \tag{3.5}$$

is the Hessian. Each iteration of equation 3.4 yields Δx_n, commonly referred to as the search direction within the context of gradient-based optimization techniques. The updated design variable is then calculated as

$$x_{n+1} = x_n + \Delta x_n \tag{3.6}$$

Newton iterations are executed until a solution x^* is found that satisfies equation 3.3 to within some user-defined tolerance.

3.2 BFGS Algorithm for Unconstrained Optimization Problems

The quasi-Newton BFGS[1] algorithm can be used to find a local minimum of an unconstrained function $\mathcal{J}$. The following sections summarize the algorithm and address the issue of constraints.

Consider a multivariate scalar function, $\mathcal{J}(X)$, where

$$X = [x_1, x_2, \ldots, x_j], \quad j \geq 2 \tag{3.7}$$

As stated in Section 3.1, Newton's method requires the gradient and inverse Hessian at each iteration to obtain the search direction ΔX_n. The Hessian is a square matrix of dimension $[j \times j]$. For problems where calculation of the Hessian is prohibitively expensive, the concept of a quasi-Newton method is distinguished by its use of a less-expensive approximation of the Hessian that requires only an evaluation of the gradient $\mathcal{G}$ and the function $\mathcal{J}$. The BFGS algorithm uses an approximation to the inverse of the Hessian, $\mathcal{M}$, to obtain the search direction ΔX_n given by

$$\Delta X_n = -\mathcal{M}_n \mathcal{G}_n \tag{3.8}$$

The update of the function variables is then calculated as

$$X_{n+1} = X_n + \beta_n \Delta X_n \tag{3.9}$$

where β is a step size determined by a line-search procedure.

The BFGS secant update is used to determine the approximation to the inverse Hessian at each iteration and is given by

$$\mathcal{M}_{n+1} = \mathcal{M}_n - \frac{\mathcal{M}_n v_n \left(\mathcal{M}_n v_n\right)^T}{v^T \mathcal{M}_n v_n} + \frac{\delta_n \delta_n^T}{\delta_n^T v_n} + v_n^T \mathcal{M}_n v_n \left(r_n r_n^T\right) \tag{3.10}$$

[1] Broyden Fletcher Goldfarb Shanno

where

$$r_n = \frac{\delta_n}{\delta_n^T v_n} - \frac{\mathcal{M}_n v_n}{v_n^T \mathcal{M}_n v_n^T} \tag{3.11}$$

and

$$\delta_n = X_{n+1} - X_n \tag{3.12}$$

$$v_n = \mathcal{G}_{n+1} - \mathcal{G}_n \tag{3.13}$$

The steepest descent direction, $-\mathcal{G}_0$, is used as the initial search direction, ΔX_0. It is obtained by setting $\mathcal{M}_0$ equal to the identity matrix. After the first step but before the first update of $\mathcal{M}$, the value of $\mathcal{M}_0$ is set to

$$\mathcal{M}_0 = \frac{v_n^T \Delta X_n}{v_n^T v_n} I \tag{3.14}$$

This formula attempts to make the size of the eigenvalues of $\mathcal{M}_0$ similar to those of the Hessian at X_0 and has been found to work well in practice [13].

At each design iteration, a line search algorithm is used to choose a step size β_n that satisfies the strong Wolfe [13] conditions given by

$$\mathcal{J}\left(X_n + \beta_n \Delta X_n\right) \leq \mathcal{J}\left(X_n\right) + c_1 \beta_n \mathcal{G}\left(X_n\right)^T \Delta X_n \tag{3.15}$$

$$\left|\mathcal{G}\left(X_n + \beta_n \Delta X_n\right)^T \Delta X_n\right| \leq c_2 \left|\mathcal{G}\left(X_n\right)^T \Delta X_n\right| \tag{3.16}$$

where $c_1 = 0.9$ and $c_2 = 1 \times 10^{-4}$. Satisfaction of the strong Wolfe conditions ensures that a reasonable approximation of the inverse Hessian is maintained over successive iterations. The step size that satisfies the strong Wolfe conditions produces a sufficient decrease in the objective function and gradient norm.

The line search algorithm begins with a step size of $\beta_0 = 1$. If the strong Wolfe conditions are not satisfied with β_0, then a new step size is calculated by finding the minimum of a cubic interpolant of the objective function along the search direction. The objective function and gradient at each line-search attempt are used to construct the cubic interpolant model.

3.2.1 Quadratic penalty method for geometric constraints

The mathematical description of the optimization problem given by equations 3.1 and 3.2 allows for consideration of constraints. The practical aerodynamic design problem investigated in this thesis includes geometric constraints on airfoil thickness that are imposed to prevent the formation of infeasible shapes such as may occur with trailing edge cross-over and to ensure structural and manufacturing design requirements are satisfied. Since the BFGS algorithm can only handle unconstrained problems, a strategy is required that allows for consideration of constraints. For the cases in this thesis that use the BFGS algorithm within Optima2D, the thickness constraints are added to the objective function as quadratic penalty terms. The formulation is given by

$$\mathcal{J} = \mathcal{J}_d + \omega_T \sum_{j=1}^{N_T} T_j \tag{3.17}$$

where $\mathcal{J}_d$ represents a design objective function, T_j are the penalty terms representing the thickness constraints, N_T is the number of thickness constraints, and ω_T is a user-defined weight applied to the penalty terms to control how well the thickness constraints are satisfied. The penalty terms, T_j, are given by

$$T_j = \begin{cases} \left[1 - h\left(x_j\right)/h^*\left(x_j\right)\right]^2 & \text{if } h\left(x_j\right) < h^*\left(x_j\right) \\ 0 & \text{otherwise} \end{cases} \tag{3.18}$$

where $h\left(x_j\right)$ is the airfoil thickness at location x_j in the chordwise direction, and $h^*\left(x_j\right)$ is the target thickness. For further information on quadratic penalty methods, see [13].

3.3 SNOPT Algorithm for Constrained Optimization Problems

The SNOPT algorithm uses a sequential quadratic programming (SQP) approach to solve non-linearly constrained optimization problems. It performs operations with constraints directly during the course of an optimization to ensure they are explicitly satisfied

at the solution, in contrast to the quadratic penalty method, which indirectly satisfies constraints by way of penalty terms in the objective function.

The SQP approach used by SNOPT obtains search directions from a sequence of quadratic programming (QP) subproblems. Each QP subproblem minimizes a quadratic model of a Lagrangian function that represents an objective function subject to constraints. Each SNOPT major iteration is the iterate from a line search that reduces a merit function along a search direction obtained from the solution of a QP subproblem. The quadratic model of the Lagrangian at each QP subproblem uses an approximation of the Lagrangian's Hessian. On completion of the line search after each QP subproblem, the approximate Hessian of the Lagrangian is updated using the BFGS secant update described in equations 3.10 - 3.13. SNOPT minor iterations are the steps required to minimize the quadratic model of the Lagrangian at each QP subproblem. The minor iteration steps are based on search directions obtained using active-set methods. For a complete description of the SNOPT algorithm, see Gill, Murray and Saunders [6].

Chapter 4

Solving Practical Aerodynamic Design Problems

4.1 Design Problem Definition

In order to define a practical aerodynamic design problem, a design specification for a hypothetical aircraft is considered[1]. The aircraft has a maximum weight of 100,000 lbs, a wing area of 1000 square feet, with a 35-degree sweep. The maximum cruise Mach number of the aircraft is 0.88. The design of the wing section at the mean aerodynamic chord is considered, and it is assumed that the sectional lift coefficient is equal to the wing lift coefficient. The target thickness to chord ratio is 0.118. Regions of the flight envelope considered for this design problem include cruise, long-range cruise, dive, and low-speed conditions.

The first four operating conditions, labeled A-D in Table 4.1, correspond to cruise. Due to the sweep angle, the effective Mach number is 0.72. Two sets of operating weights and altitudes are considered. For operating point A the altitude is 29,000 feet, the weight is 60,000 lbs.; for B the altitude is the same, but the weight is 100,000 lbs.; for C the

[1]The design specification was provided by Dr. Tom Nelson at Bombardier Aerospace

Operating Point	Reynolds Number	Mach Number	Lift Coefficient
A	27.32×10^6	0.72	0.17
B	27.32×10^6	0.72	0.28
C	18.57×10^6	0.72	0.27
D	18.57×10^6	0.72	0.45
E	24.22×10^6	0.64	0.21
F	24.22×10^6	0.64	0.36
G	16.46×10^6	0.64	0.34
H	16.46×10^6	0.64	0.57
I	28.88×10^6	0.76	0.28
J	28.88×10^6	0.76	0.15
K	28.88×10^6	0.76	0.46
L	28.88×10^6	0.76	0.25
M	19.62×10^6	0.76	0.45
N	19.62×10^6	0.76	0.24
O	19.62×10^6	0.76	0.74
P	19.62×10^6	0.76	0.40
Q	11.8×10^6	0.16	-
R	15.0×10^6	0.20	-

Table 4.1: Operating conditions for an 18-point optimization

Operating Point	Operating Condition	On-Design Objective	Off-Design Constraint
A-D	cruise	lift-constrained drag minimization	-
E-H	long-range cruise	lift-constrained drag minimization	-
I-P	dive	-	$M_{\max} \leq 1.35$
Q-R	low-speed	-	$C_{\mathrm{l,max}} \geq 1.60$

Table 4.2: Design objectives and constraints for an 18-point optimization

altitude is 39,000 feet, the weight is 60,000 lbs.; for D the altitude is 39,000 feet, the weight is 100,000 lbs. This leads to the Reynolds numbers and lift coefficients given in Table 4.1.

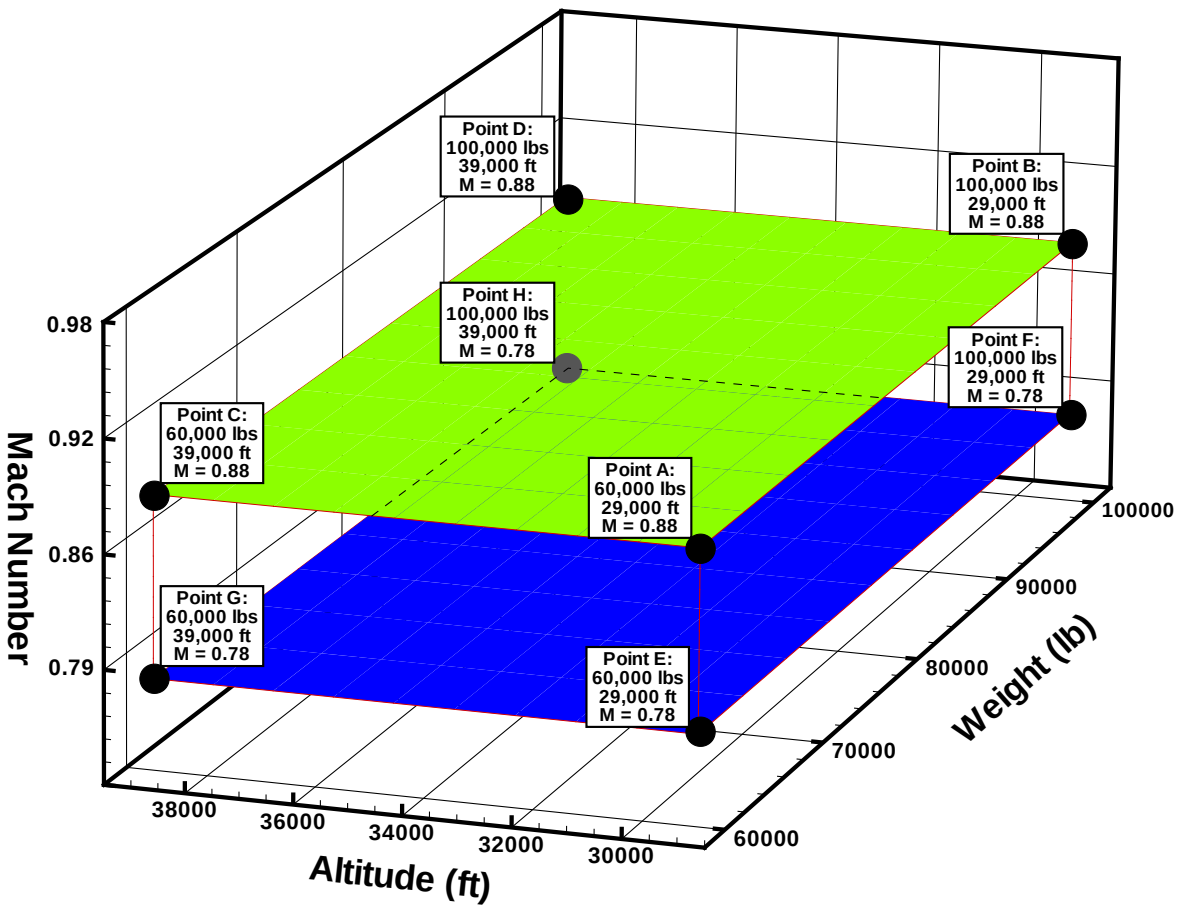

Figure 4.1: Visualization of cruise and long-range cruise operating conditions (used with permission from B. Y. Zhou [24])

The next four operating conditions, labeled E-H, correspond to long-range cruise. The Mach number is 0.78, producing an effective Mach number of 0.64. The altitudes and weights are the same as for A-D respectively. The green and blue surfaces shown in Figure 4.1 provide a graphical representation of the cruise and long-range cruise operating conditions, respectively.

The cruise and long-range cruise conditions represented by design points A-H are considered *on-design* operating conditions. The on-design performance goal for these

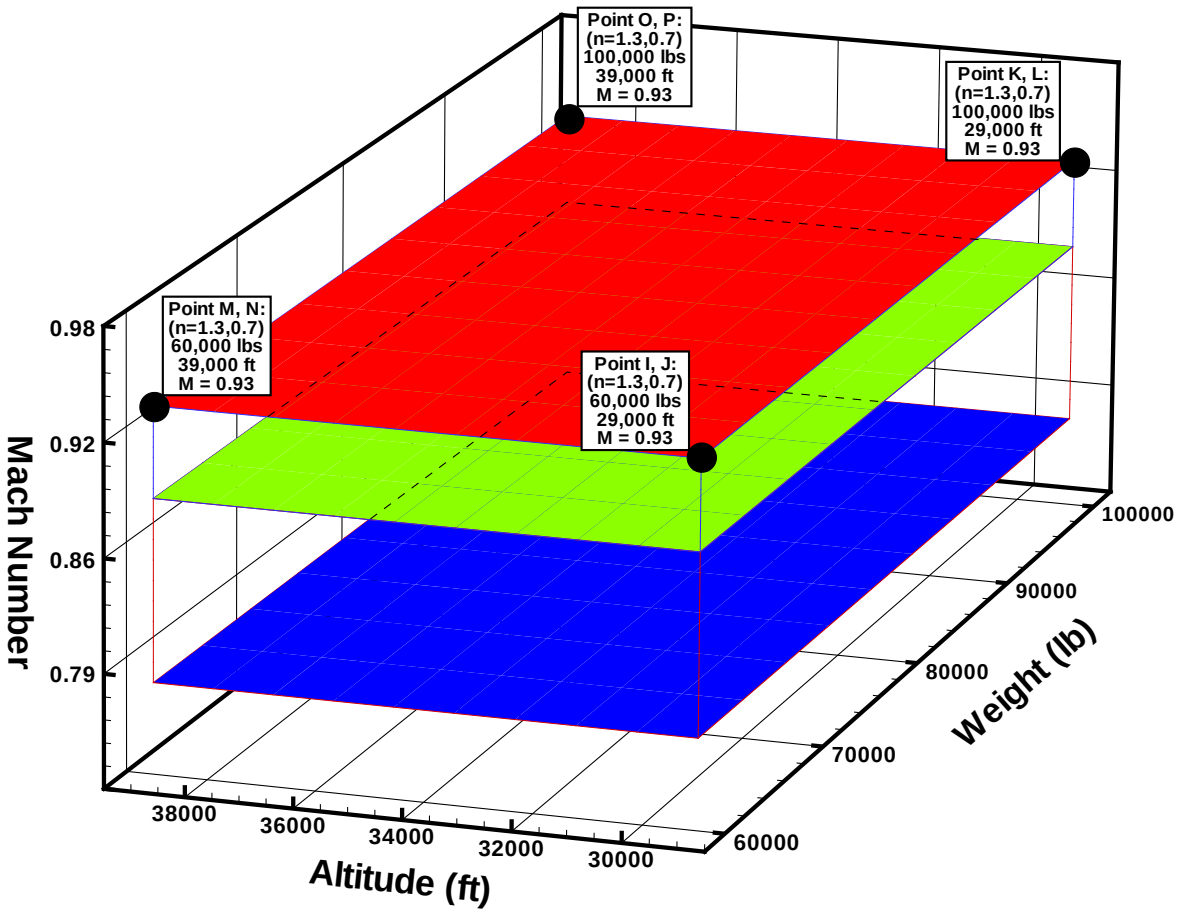

Figure 4.2: Visualization of dive operating conditions (used with permission from B. Y. Zhou [24])

eight design points is to minimize drag while maintaining their specified lift coefficients. A complete problem specification could involve a careful prioritization by the designer of these operating conditions based on the knowledge of the aircraft mission requirements. In the present design problem specification, all on-design points are assigned equal importance.

The next eight operating conditions (I-P) are associated with a safety requirement for maneuverability under dive conditions. The flight Mach number is 0.93, making

the effective Mach number 0.76. In addition to the two sets of weights and altitudes considered for the on-design points, two load factors are also taken into account. The combination produces a total of eight dive operating conditions. For operating point I, the altitude is 29,000 ft., the weight 60,000 lbs., and the load factor is 1.3. For operating point J, the altitude and weight are the same, but the load factor is 0.7. Operating points K and L have an altitude of 29,000 ft., a weight of 100,000 lbs., and load factors 1.3 and 0.7, respectively. For operating points M and N, the altitude is 39,000 ft., the weight is 60,000 lbs., and the load factors are 1.3 and 0.7, respectively. Operating points O and P have the same altitude and load factors, but the weight is 100,000 lbs. The dive maneuverability requirement is achieved by keeping shock strengths modest under these conditions, such that the upstream Mach number at all shocks is less than or equal to 1.35. The red surface shown in Figure 4.2 provides a graphical representation of the dive operating conditions.

The final two operating points reflect a safety requirement to be able to achieve an adequate maximum lift coefficient at low speed conditions. For operating condition Q, the altitude is sea level, the weight is 60,000 lbs., and the effective Mach number is 0.16. For operating point R the weight is 100,000 lbs., and the effective Mach number is 0.20. The safety requirement specifies that the maximum attainable lift coefficient under these conditions is at least 1.75[2].

The last ten design points, I-R, represent *off-design* operating conditions. The design requirements at these conditions impose constraints on the optimization. These eighteen operating points span the flight envelope. Table 4.2 summarizes the design objectives and constraints for this design problem. This design problem definition is meant to illustrate a basic set of on-design and off-design specifications that can be used to formulate a multipoint optimization problem. In practice, additional operating conditions, such as

[2]The optimization procedures applied to this design problem are demonstrated on a coarse mesh. Prior experience has shown that using a lower target lift coefficient of 1.60 on our coarse mesh will yield a lift coefficient of at least 1.75 on a finer mesh.

climb, also need to be considered, but can be easily accommodated by the methods presented in this thesis.

4.2 A Strategy For Obtaining Ideal Weights For Off-Design Points (Method 1)

Practical aerodynamic design problems as defined in this thesis are by nature constrained optimization problems. The composite objective function used in this method written in terms of on-design and off-design points is given by

$$\mathcal{J} = \sum_{p=1}^{\substack{\#\text{ of}\\ \text{on-design}}} \omega_p \mathcal{J}_p \quad + \quad \sum_{q=1}^{\substack{\#\text{ of}\\ \text{off-design}}} \omega_q \mathcal{J}_q \tag{4.1}$$

The goal of the strategy used in this method is to find the values for the off-design weights, ω_q, that allow the best possible on-design performance to be achieved while satisfying the off-design constraints. These ideal off-design weights are obtained using an automated weight update procedure that exploits aerodynamic performance trends as they evolve throughout the optimization. The strategy presented in this section employs the unconstrained BFGS optimization algorithm described in Section 3.2.

The objective function used at on-design points A-H and off-design points I-P is $\mathcal{J} = C_d$. The lift requirements for these points specified in Table 4.1 are satisfied using the technique described by Billing [2] whereby the angle of attack is altered during the iterations of the flow solution such that the desired value of C_l is obtained at convergence. The design variable vector X for this objective function contains only geometric design variables (B-spline control points that define the airfoil geometry).

It is important to note that the off-design constraints are represented as objective functions in this method, as shown in equation 4.1, because they cannot be handled directly by the BFGS algorithm. The off-design constraints are satisfied indirectly by

minimizing objective functions known to correlate with the constraint values. For example, the off-design constraints at operating points I-P are given by $M_{\max} \leq 1.35$. The upstream Mach number near a shock on the airfoil has a loose correlation to the drag coefficient. By reducing the drag coefficient, the maximum Mach number in the flow field is also reduced. Therefore, the objective function representing these off-design constraints is given by $\mathcal{J} = C_d$. At off-design points where $M_{\max} > 1.35$, the corresponding off-design weights are adjusted so that C_d is reduced just enough to satisfy the $M_{\max}$ constraint value at exactly 1.35.

The same logic is applied to the high-lift constraints at off-design points Q and R where the constraints are given by $C_{\text{l,max}} \geq 1.60$. In this case, the objective function representing these constraints is given by

$$\mathcal{J} = \left(1 - \frac{C_{\text{l,max}}}{\widehat{C}^*_{\text{l,max}}}\right)^2 \tag{4.2}$$

where $\widehat{C}^*_{\text{l,max}}$ is a target maximum lift coefficient specific to the objective function not to be confused with the desired target maximum lift coefficient $C^*_{\text{l,max}}$ (see equation 4.6 used in the weight update formula). The value of $\widehat{C}^*_{\text{l,max}}$ is set to a value that is unattainable and hence this corresponds to lift maximization. The optimization algorithm will strive to attain the objective-function-specific target lift value $\widehat{C}^*_{\text{l,max}}$ at points Q and R while their corresponding weights will be adjusted to ensure that the desired target lift value $C^*_{\text{l,max}}$ is obtained. For this lift maximization objective function, the angle of attack, α, is a design variable in addition to the geometric design variables.

In a sense, the weight update strategy attempts to emulate the behaviour of a constrained optimization algorithm. The off-design weight update strategy was the first of two methods developed for practical aerodynamic design problems. This approach was pursued in order to take advantage of the strong legacy of work and experience supporting the BFGS optimization algorithm within Optima2D.

4.2.1 On-design-first optimization

In this approach, the procedure begins with an optional start-up optimization. The term on-design-first refers to this start-up optimization, which includes only the on-design points. The composite objective function used for the on-design-first optimization is given by

$$\mathcal{J} = \sum_{p=1}^{\substack{\#\text{ of} \\ \text{on-design}}} \omega_p \mathcal{J}_p \tag{4.3}$$

Performing an initial optimization with only on-design operating points serves two purposes. First, the initial airfoil may be poorly suited to the off-design operating points, which may cause flow solver convergence difficulties. In such cases, performing the on-design-first optimization typically provides a better starting shape for introducing the off-design points. Second, it gives a clear picture of the performance trade-offs associated with the off-design constraints. The resultant airfoil geometry from the on-design-first optimization minimizes a weighted sum of the objective functions at all on-design points given by equation 4.3. Under the assumption that all of the on-design operating conditions are of equal importance, all on-design objective functions are weighted equally; however the weight assignment is ultimately at the discretion of the designer, who may choose to weight the on-design points differently according to design priorities. This on-design-first airfoil is the starting point for the main optimization procedure that includes both the on-design points and the off-design points.

In cases where the initial airfoil geometry does not cause flow solver convergence difficulties at any of the off-design points, the on-design-first optimization is not necessary. Moreover, the method is more efficient if the on-design first optimization can be omitted as shown by the results presented in Section 5.

Treatment of leading edge geometry

For cases where an on-design-first optimization is necessary, a special treatment of the airfoil leading edge is required. In the absence of constraints at off-design points Q and R

representing high lift requirements, an on-design-first optimization with the performance goal of drag minimization will produce an airfoil leading edge with a very small radius of curvature approaching a sharp point. This is problematic because flow-solver difficulties will likely be encountered when the off-design points are introduced, in particular at the high-lift points. This situation can be avoided by freezing the control point at the leading edge as well as the control points above and below the control point at the leading edge, which has the effect of preserving the leading edge geometry from the initial airfoil throughout the on-design-first optimization. After the on-design-first optimization, the control points above and below the leading edge are un-frozen during the off-design weight update procedure. It is due to the presence of the high-lift points that the leading edge geometry remains feasible during this stage since any thinning of the leading edge would counteract the optimizer's effort to increase lift.

4.2.2 Weight update formula

For any given off-design point, there are 3 possibilities for the value of its respective aerodynamic constraint:

1. Constraint is violated
2. Constraint is exactly satisfied
3. Constraint is over-satisfied

For off-design points where the aerodynamic constraints are violated, a higher weight is required on these points to pull them into the feasible region of the design space. For off-design points where the aerodynamic constraints are exactly satisfied, the weight is appropriate and does not require modification. For off-design points where constraints are over-satisfied, a lower weight is required to allow them to drift toward the boundary of the feasible region of the design space. As there is no particular benefit to over-satisfying

an off-design aerodynamic constraint, it is desirable to shed weight on the off-design points that are in this category to reduce the negative impact on on-design performance. To facilitate the modification of off-design weights, a simple weight update formula is employed.

The concept for this approach to off-design weight modification can be credited to the work of Zingg and Elias [25] that demonstrates a similar technique for obtaining equal drag coefficients across a range of cruise Mach numbers by altering the objective function weights of design points in a multipoint optimization. For an aerodynamic constraint given by $\psi \leq \psi^*$, where ψ is some functional, the weight update formula used in this procedure is:

$$\omega_{n+1} = \omega_n \left(\frac{\psi_n}{\psi^*} \right)^h \tag{4.4}$$

where ψ_n is the current off-design aerodynamic constraint value, ω_n and ω_{n+1} are the current and updated off-design point weights, the exponent h is a user defined parameter that affects the magnitude of the weight change, and n is the index of weight update cycles.

For off-design points representing requirements for $C_{\mathrm{l,max}}$, the values of ψ_n and ψ^* to be used in the weight update formula are:

$$\psi_n = \frac{1}{C^n_{\mathrm{l,max}}} \tag{4.5}$$

$$\psi^* = \frac{1}{C^*_{\mathrm{l,max}}} \tag{4.6}$$

For off-design points with a maximum local Mach number constraint, $M_{\mathrm{max}} \leq M^*_{\mathrm{max}}$, the values of ψ_n and ψ^* to be used in the weight update formula are defined in equations 4.7 and 4.8 respectively.

$$\psi_n = M^n_{\mathrm{max}} \tag{4.7}$$

$$\psi^* = M^*_{\mathrm{max}} \tag{4.8}$$

The first application of the weight update formula to obtain initial off-design weights ω_1 requires special treatment because there are no previous weights to use in the formula.

An arbitrary value of unity is assigned to ω_0 for all off-design points. The off-design constraint values ψ_0 are evaluated using the initial airfoil geometry (or the on-design-first airfoil geometry in some cases). Initial off-design weights ω_1 are then calculated using the weight update formula with $\omega_0 = 1$. It is important to clarify that the ω_0 weights are not used at any time during the optimization procedure; they only facilitate the calculation of ω_1. The weight update formula is subsequently used at regular intervals (after every weight update cycle) throughout the main optimization procedure to update the off-design point weights.

4.2.3 Angle of attack sweep to obtain $C_{\mathrm{l,max}}$

For a given high-lift off-design point, the angle of attack, α, used during the last optimization iteration of a weight update cycle does not necessarily produce the $C_{\mathrm{l,max}}$ value attainable at that airfoil geometry. An α that produces $C_{\mathrm{l,max}}$ is only guaranteed at a solution that minimizes the high-lift objective function given by equation 4.2; i.e. at the converged solution. Since the solution at the end of a given weight update cycle is not necessarily converged, a method is required to obtain an α that produces a better estimate of $C_{\mathrm{l,max}}$ at each high-lift point for calculation of the constraint ψ_n defined in equation 4.5. During the early weight update cycles when the solution is far from converged, the need for such a method is greater than during the later weight update cycles. To obtain an α that produces a better estimate of $C_{\mathrm{l,max}}$, an angle of attack sweep is performed using the airfoil geometry from last optimization iteration of the current weight update cycle. Given that a costly flow solution is required for each data point in an angle of attack sweep, the method presented in this section is designed to efficiently identify the value α^* that attains $C_{\mathrm{l,max}}$ such that the minimum number of flow solutions are required.

There are three possible C_l scenarios corresponding to the angle of attack value used during the last optimization iteration of a weight update cycle, α_0:

1. $\alpha_0 = \alpha^*$. $C_{\mathrm{l,max}}$ is attained at α_0

2. $\alpha_0 < \alpha^*$. C_l is increasing for values of $\alpha > \alpha_0$

3. $\alpha_0 > \alpha^*$. C_l is decreasing for values of $\alpha > \alpha_0$

Figure 4.3 illustrates these scenarios respectively. To determine which scenario is applicable, C_l is evaluated at $\alpha_0 + \Delta\alpha$ and $\alpha_0 - \Delta\alpha$. If $C_l(\alpha_0 - \Delta\alpha) < C_l(\alpha_0) > C_l(\alpha_0 + \Delta\alpha)$ then scenario 1 has been identified ($\alpha_0 = \alpha^*$). In this case α_0 gives a good estimate of $C_{\mathrm{l,max}}$; therefore set $C_{\mathrm{l,max}} = C_l(\alpha_0)$ and return to the calculation of the high-lift constraint ψ_n. If $C_l(\alpha_0 - \Delta\alpha) < C_l(\alpha_0) < C_l(\alpha_0 + \Delta\alpha)$ then scenario 2 has been identified ($\alpha_0 < \alpha^*$). In this case, α_0 is successively incremented by $\Delta\alpha$ until $C_{\mathrm{l,max}}$ is bracketed as in scenario 1; then return to the calculation of the high-lift constraint. Finally, if $C_l(\alpha_0 - \Delta\alpha) > C_l(\alpha_0) > C_l(\alpha_0 + \Delta\alpha)$ then scenario 3 has been identified ($\alpha_0 > \alpha^*$). In this case α_0 is successively decremented by $\Delta\alpha$ until $C_{\mathrm{l,max}}$ is bracketed as in scenario 1; then return to the calculation of the high-lift constraint.

4.2.4 Weight update cycles

The weights of the off-design points are updated periodically based on the values of their respective aerodynamic constraints during the course of the optimization. A weight update cycle consists of a user-specified number of optimization iterations followed by an angle of attack sweep to determine values of $C_{\mathrm{l,max}}$ for the high-lift points, and finally an evaluation of the off-design aerodynamic constraints with a corresponding update of the off-design weights. A new weight update cycle begins with a restarted optimization using the updated off-design weights and the final airfoil geometry from the previous weight update cycle. If the magnitude of the change in the updated weights is less than a user-specified tolerance, the optimization leaves the weights unchanged and continues until the next weight update cycle. In this manner, weight update cycles are executed until a converged optimal solution is obtained. At the converged optimal solution, the

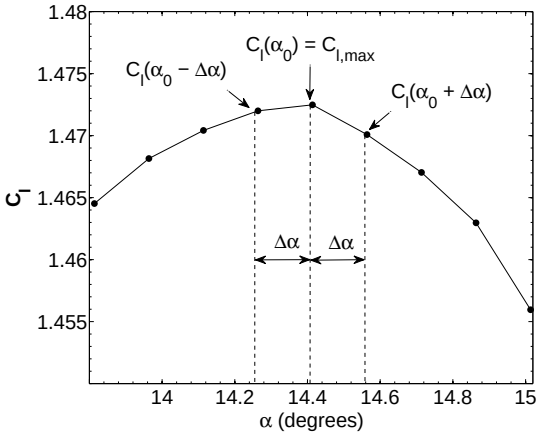

(a) Scenario 1 ($\alpha_0 = \alpha^*$)

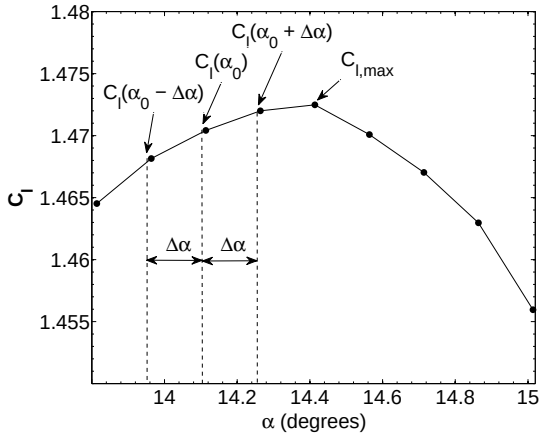

(b) Scenario 2 ($\alpha_0 < \alpha^*$)

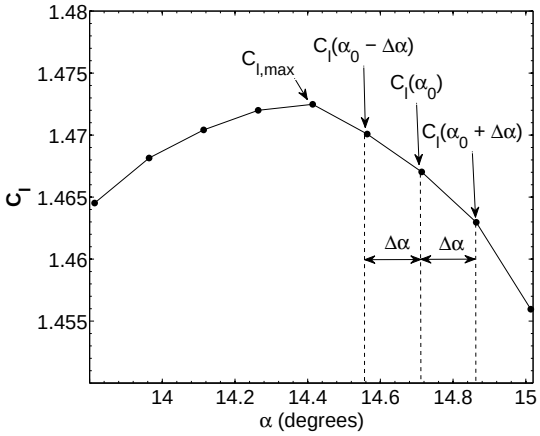

(c) Scenario 3 ($\alpha_0 > \alpha^*$)

Figure 4.3: $C_{\mathrm{l,max}}$ Scenarios For Angle of Attack Sweep

off-design weights are as low as possible while satisfying all of the off-design aerodynamic constraints.

4.3 An Alternative Strategy Using Constrained Optimization (Method 2)

An alternative strategy for solving practical aerodynamic design problems utilizes the SNOPT algorithm for constrained optimization problems developed by Gill, Murray and

Saunders [6]. The SNOPT algorithm allows us to treat the off-design operating conditions as explicit constraints within the framework of a constrained optimization problem. SNOPT uses a sequential quadratic programming (SQP) method that obtains search directions from a sequence of quadratic programming (QP) subproblems. Each QP subproblem minimizes a quadratic model of a Lagrangian function which is used to represent an objective function subject to inequality constraints.

The Lagrangian function in terms of a practical aerodynamic design problem is given by

$$\mathcal{L}(X, \widehat{Q}, \pi, \lambda) = \sum_{p=1}^{\substack{\#\text{ of} \\ \text{on-design}}} \omega_p \mathcal{J}_p(X, \widehat{Q}) - \sum_{q=1}^{\substack{\#\text{ of} \\ \text{off-design}}} \pi_q C_q(X, \widehat{Q}) - \sum_{r=1}^{N_G} \lambda_r^* C_r(X) \tag{4.9}$$

where the first term is a weighted sum of on-design objectives. The second and third terms are weighted sums of off-design constraints and geometric constraints, respectively. The objective function used at on-design points A-H is $\mathcal{J} = C_d$. A maximum Mach number constraint function is used at off-design points I-P, and a high-lift constraint function is used at off-design points Q and R. The lift requirements specified at on-design points A-H and off-design points I-P are achieved using Billings' method [2] whereby the angle of attack is altered during the iterations of the flow solution such that the desired value of C_l is obtained at convergence. Note that the off-design constraints are functions of performance values, $M_{\max}$ and $C_{\text{l,max}}$, obtained from flow solutions, $\widehat{Q}$, at their respective operating conditions, whereas the geometric constraints are solely a function of the geometric design variables contained within X.

The significant distinction between this approach to solving practical aerodynamic design problems and the off-design weight update approach described in Section 4.2 is that the SNOPT algorithm performs operations with constraints directly during the course of an optimization to ensure they are explicitly satisfied at the solution, in contrast to the off-design weight update approach which indirectly satisfies constraints by reducing objective functions known to correlate with constraint values. The SNOPT algorithm seeks to

satisfy the first-order optimality conditions for a constrained optimization problem, also known as the Karush-Kuhn-Tucker (KKT) conditions [13]. The KKT conditions that define an optimal solution, $(X^*, \widehat{Q}^*, \pi^*, \lambda^*)$, to the Lagrangian defined in equation 4.9 are given by

$$\nabla_{\mathrm{x}}\mathcal{L}(X^*, \widehat{Q}^*, \pi^*, \lambda^*) = 0 = \sum_{p=1}^{\substack{\#\text{ of}\\ \text{on-design}}} \omega_p \nabla \mathcal{J}_p(X^*, \widehat{Q}^*) - \sum_{q=1}^{\substack{\#\text{ of}\\ \text{off-design}}} \pi_q^* \nabla C_q(X^*, \widehat{Q}^*) - \sum_{r=1}^{N_G} \lambda_r^* \nabla C_r(X^*) \tag{4.10}$$

and

$$C_q(X^*, \widehat{Q}^*) \geq 0, \quad \text{for all } q \in [\text{off-design constraints}] \tag{4.11}$$

$$\pi_q^* \geq 0, \quad \text{for all } q \in [\text{off-design constraints}] \tag{4.12}$$

$$\pi_q^* C_q(X^*, \widehat{Q}^*) = 0, \quad \text{for all } q \in [\text{off-design constraints}] \tag{4.13}$$

$$C_r(X^*) \geq 0, \quad \text{for all } r \in [\text{geometric constraints}] \tag{4.14}$$

$$\lambda_r^* \geq 0, \quad \text{for all } r \in [\text{geometric constraints}] \tag{4.15}$$

$$\lambda_r^* C_r(X^*) = 0, \quad \text{for all } r \in [\text{geometric constraints}] \tag{4.16}$$

The conditions 4.13 and 4.16 are the complementarity conditions for the off-design constraints and the geometric constraints, respectively. They imply that the Lagrange multipliers, π_q^* and λ_r^*, corresponding to inactive off-design and geometric constraints are zero, respectively. It is interesting to note that the off-design weights, ω_q, of Method 1 exhibit similar behaviour to the Langrange multipliers for the off-design constraints, π_q^*, in that the values of ω_q^* at the solution are also zero at off-design points with inactive constraints. This observation is highlighted in the results presented in Section 5.5

4.3.1 On-design-first optimization with SNOPT

As with the off-design weight update strategy, it may be necessary to perform an on-design-first optimization to obtain a favourable airfoil geometry for use as a starting

point before the introduction of the off-design constraints. In such cases SNOPT is used to minimize a weighted sum of the objective functions at all on-design points. This composite objective function is subject only to geometric thickness constraints which are satisfied explicitly by SNOPT. The same leading edge treatment described in Section 4.2.1 is applied in this case.

4.3.2 *KS* function used for evaluation of maximum Mach number constraints

Off-design points I-P representing dive conditions are subject to the constraint that the maximum Mach number in the flow field not exceed 1.35. B-spline control points are used as design variables for the maximum Mach number constraint function. This function is not continuous with respect to the design variables and therefore cannot be handled directly by SNOPT. This is because SNOPT assumes continuity in the first and second derivatives of the objective and constraint functions used in the construction of the quadratic model of the Lagrangian at each major iteration. A change in the design variables may cause a change in the nodal location of the maximum Mach number and a discontinuous jump in the corresponding Mach number at the new location. Since the Mach number at each node is continuous with respect to the design variables, a Mach number constraint could be assigned to each node in the flow field. However, performing an adjoint gradient evaluation of the Mach number constraint at each node would be prohibitively expensive. Instead, the Kreisselmeier-Steinhauser (KS) function is used as a means to aggregate the Mach number constraints at all nodes in the flow field into a single composite function that is continuously differentiable. The KS function produces an envelope surface that is C_1 continuous and represents a conservative estimate of the maximum among the set of constraint functions considered [22]. The KS function has been used in various applications where constraint aggregation is required for efficient use of gradient-based optimization methods including aerodynamic shape optimization [1]

and aircraft design [20, 9, 16]. An alternate formulation of the KS function proposed by Wrenn [22] is used to reduce numerical difficulties associated with the original formulation and is given by

$$KS[g(X)] = g_{\max}(X) + \frac{1}{\rho}\ln\left[\sum_{j=1}^{m} e^{\rho[g_j(X)-g_{\max}(X)]}\right] \tag{4.17}$$

where $g(X)$ contains the set of constraints, $g_{\max}$ is the maximum constraint value evaluated at the current design iteration, X, and ρ is the *draw-down* parameter that governs the conservativeness of the estimate of $g_{\max}$ such that

$$\lim_{\rho\to\infty} KS(X,\rho) = g_{\max}(X) \tag{4.18}$$

The constraints $g_j(X)$ are evaluated at every node in the flow field with the exception of the nodes on the surface of the airfoil and are given by:

$$g_j(X) = \frac{M_j(X)}{M^*} - 1 \tag{4.19}$$

where $M^* = 1.35$ is the upper bound on the Mach number constraint, $M_j(X)$ is the Mach number at node j at the current design iteration, and the constraint is considered satisfied if $g_j(X) \leq 0$. The maximum constraint value, $g_{\max}$, is given by:

$$g_{\max}(X) = \frac{M_{\max}(X)}{M^*} - 1 \tag{4.20}$$

where $M_{\max}(X)$ is the maximum Mach number in the flow field at the current design iteration.

A conservative estimate of the maximum Mach number is given by:

$$M_{\text{ks}}(KS) = (KS+1)M^* \tag{4.21}$$

The actual constraint that SNOPT works with is M_{ks}. To obtain a solution that satisfies the desired maximum Mach number constraint, M^*, appropriate values of ρ and the M_{ks} target must be specified and are case dependent. Currently, an ad-hoc approach is taken to determine these values. See Section 5.5 for a description of this approach.

4.3.3 Evaluation of high-lift constraints

Off-design points Q-R representing design requirements for high lift at low speeds are subject to the constraint that $C_{\mathrm{l,max}}$ must be at least 1.60. The constraint function assigned to these points is given simply as C_l. For this high-lift constraint function, the angle of attack is a design variable in addition to the geometric design variables.

4.3.4 Off-design constraint function gradients

The gradients of the constraint functions M_{ks} and C_l with respect to the design variables, X, are computed using the discrete adjoint approach. To make use of the existing adjoint gradient evaluation capabilities of Optima2D described in Section 2.5, new definitions for the partial derivatives $\frac{\partial \mathcal{J}}{\partial \widehat{Q}}$ and $\frac{\partial \mathcal{J}}{\partial X}$ have been created for the off-design constraint functions M_{ks} and C_l. The partial derivative $\frac{\partial \mathcal{J}}{\partial \widehat{Q}}$ is calculated analytically for both constraint functions, while $\frac{\partial \mathcal{J}}{\partial X}$ is calculated using finite differences for the C_l constraint function. Since the Mach number at any given node has no direct sensitivity to the design variables, X, $\frac{\partial \mathcal{J}}{\partial X} = 0$ for the M_{ks} constraint function.

4.4 Parallel Computing Implementation

For practical aerodynamic design problems, the vast majority of the computational effort is devoted to solving the governing flow equations and the adjoint equation for gradient calculations at each operating condition considered in the multipoint optimization. The computational effort increases at a linear rate with the number of operating conditions required to represent the design problem. Previously, Optima2D only had the capability to perform serial multipoint optimizations. For serial multipoint optimizations, one processor is used to perform calculations at all operating conditions. At each design iteration, a flow solve and gradient calculation is performed for each operating condition, one at a time. After evaluation of all operating conditions has been completed, the com-

posite objective function and composite gradient are formed. In a serial implementation of a practical aerodynamic design problem, as with the computational effort, the time required also increases linearly with the number of operating conditions. For design problems with many operating conditions, such as the problem described in Section 4.1, the time required to obtain a solution using a serial implementation is a major imposition.

To overcome excessive time requirements associated with serial multipoint optimizations, a parallel version of Optima2D has been developed specifically to handle large multipoint optimizations. The parallel implementation assigns a dedicated processor to each operating condition in a multipoint optimization. The flow solves and gradient calculations at N operating conditions are all calculated at the same time on N processors. While the computational effort for the parallel implementation remains the same as for the serial implementation, the time requirements are independent of the number of operating conditions, rendering large multipoint optimizations surmountable.

Chapter 5

Results

The results presented in this section demonstrate the application of both methods to the practical aerodynamic design problem described in Section 4.1. A variety of cases are used to validate the methods as well as illustrate similarities and differences between them.

5.1 Multipoint Optimization Setup

For all cases, the airfoil geometry is parametrized using 15 B-spline control points. Three control points are frozen at the leading edge and two at the trailing edge. The remaining 10 control points are designated as design variables and are split evenly between the top and bottom airfoil surfaces. A floating thickness constraint of 11.9% chord is imposed to ensure a thickness of at least 11.8% chord. In addition, thickness constraints of 1% chord and 0.2% chord are imposed at 95% chord and 99% chord respectively to prevent trailing edge crossover. The latter is typically inactive once convergence is achieved. The meshes used have a C topology with 289 nodes in the streamwise direction and 65 nodes in the normal direction; the off-wall spacing is 2×10^{-6} chord. The values of the second and fourth order artificial dissipation coefficients are $\kappa_2 = 0.0$ and $\kappa_4 = 0.02$ respectively. Second order artificial dissipation is not used because it significantly reduces the acuracy

of the adjoint gradient calculation. Further discussion of this issue is provided in Section 6.1.4. Cases 1 to 3 use the off-design weight update method described in Section 4.2. Case 4 uses the constrained optimization method described in Section 4.3. The Optima2D input files used for these cases are included in Appendix A.

5.1.1 Off-design weight update setup for Cases 1 - 3

For design points A through P, the design objective is lift-constrained drag minimization. For each of these design points, the corresponding objective function is given by $\mathcal{J} = C_d$. For design points Q and R, the design objective is to meet minimum $C_{\mathrm{l,max}}$ requirements needed at low speeds. A value of 2.0 is used for $\widehat{C}^*_{\mathrm{l,max}}$ in the high-lift objective function 4.2. Off-design objective functions at design points I - R are used to satisfy corresponding off-design constraints as described in Section 4.2. The objective functions at all design points are normalized by their respective objective function values obtained using the initial airfoil geometry. The weights for the on-design points A - H remain fixed at unity throughout the duration of the optimization procedure. The weights for the off-design points I - R are periodically modified throughout the optimization procedure according to the strategy described in Section 4.2. Ten optimization iterations are executed per weight update cycle. The value of the exponent used in the weight update formula, equation 4.4, is $h = 4$.

5.1.2 Determination of parameter values for *KS* constraint function

The results presented in this section illustrate the procedure used to determine the values of ρ and M^*_{ks} used in Case 4.

Table 5.1 compares evaluations of M_{ks} to M_{max} at point O performed on the initial airfoil geometry of Case 4 at several values of ρ. It can be seen that the spread between

$M_{\mathbf{max}}$	$M_{\mathbf{ks}}$	ρ
1.45	1.74	40
1.45	1.60	60
1.45	1.50	80
1.45	1.47	100

Table 5.1: A comparison of M_{ks} to M_{max} at point O for various values of ρ

$M_{\mathbf{max}}$	$M^*_{\mathbf{ks}}$	ρ
1.40	1.50	40
1.38	1.50	37
1.36	1.50	34
1.35	1.50	31
1.32	1.50	28
-	1.50	25

Table 5.2: The effect of varying ρ on the value of M_{max} at point O at the converged solution

$M_{\mathbf{max}}$	$M^*_{\mathbf{ks}}$	ρ
1.43	1.52	40
1.42	1.51	40
1.40	1.50	40
1.38	1.49	40
-	1.48	40
-	1.47	40

Table 5.3: The effect of varying M^*_{ks} on the value of M_{max} at point O at the converged solution

M_{ks} and M_{max} decreases as ρ is increased. As stated in equation 4.18, M_{ks} is expected to approach M_{max} in the limit as ρ approaches infinity. However, in practice, there is an upper bound on ρ because it becomes increasingly difficult to obtain estimates of second derivatives of the KS function at values of X where constraints intersect. At such

locations, the curvature of the *KS* function can be very large for large values of ρ. See [16] for further details. The target value M_{ks}^* is used by SNOPT as the upper bound on the constraint function. SNOPT will ensure that $M_{\text{ks}} \leq M_{\text{ks}}^*$ at the final converged solution. A trial and error approach was used to find the right combination of M_{ks}^* and ρ to produce $M_{\text{max}} = 1.35$ at all off-design points where the M_{max} constraint is active at the final optimized solution. Table 5.2 shows the value of M_{max} for off-design point O[1] at the converged solution obtained with different values of ρ while keeping M_{ks}^* constant. Similarly, Table 5.3 shows the effect of varying M_{ks}^* while keeping ρ constant. As ρ is decreased, the spread between M_{ks} and M_{max} becomes larger, so the effect of lowering the value of ρ at a constant value of M_{ks}^* results in a lower value of M_{max}. Conversely, for a fixed value of ρ, the spread between M_{ks} and M_{max} remains roughly constant, so the value of M_{max} moves in lockstep with M_{ks}^*. Blank entries for M_{max} indicate that the optimization did not achieve a converged solution. It appears that for this case there are lower limits on M_{ks}^* and ρ below which SNOPT cannot obtain a converged solution. These results show that the combination of $M_{\text{ks}}^* = 1.50$ and $\rho = 31$ is appropriate for obtaining $M_{\text{max}} = 1.35$ at point O. It should be noted that the adaptive *KS* approach proposed by Poon and Martins [16] may provide an alternative strategy to the trial and error method presented in this section that eliminates the guess work involved in determining M_{ks}^* and ρ. Further discussion of this approach is provided in Section 6.1.2

5.1.3 Constrained optimization setup for Case 4

For on-design points A-H, the design objective is lift-constrained drag minimization. For each of these design points, the corresponding objective function is the drag coefficient normalized by the drag coefficient evaluated using the initial airfoil geometry. A composite objective function is formed by a weighted sum of the individual on-design objective functions with all weights equal to unity. The off-design constraints are defined as de-

[1]The M_{max} constraints at all other off-design points are inactive at the converged solution.

scribed in Section 4.3. A value of $\rho = 31$ is used in the KS function. The target value of M_{ks} used by SNOPT is 1.50. This produces $M_{\text{max}} \leq 1.35$ as desired.

5.2 Case 1 - Baseline 18 Point Optimization

The initial geometry used for the optimization in this case is the RAE 2822 airfoil. The full set of 18 design points, A-R, described in Table 4.1 are used.

The results presented here were obtained after 33 weight update cycles. The optimization was terminated at 33 weight update cycles when it was observed that the change in on-design drag values from cycle to cycle was significantly less than the numerical error in drag values expected from the coarse mesh used in this study. Figure 5.1 shows the optimized airfoil from Case 1 compared to the initial RAE 2822 airfoil. Tables 5.4, 5.5, and 5.6 provide a summary of the on-design and off-design performance values for the initial RAE 2822 airfoil, the on-design-first airfoil, and the airfoil after 33 weight update cycles. For the on-design-first airfoil and the optimized airfoil after 33 weight update cycles, the tabulated performance results were obtained from regenerated meshes with the same properties as the original mesh for greater accuracy[2]. Note that for the RAE 2822 airfoil the off-design constraints at points O, Q, and R, shown in red, are violated. After the on-design-first optimization, the off-design constraints at points O, Q, and R, are still violated. The final optimized airfoil for Case 1 has roughly maintained the drag coefficient values at the eight on-design points compared to the initial RAE 2822 airfoil while satisfying all off-design constraints. A comparison of the drag coefficients at the on-design points for the final optimized airfoil versus the on-design-first airfoil shows that there has been degradation in performance, but the severity of the degradation has been mitigated by use of the automated weight update procedure. Pressure distributions for

[2]During the course of an optimization if the shape of the airfoil has changed significantly from the initial geometry, degradation in the quality of the mesh is caused by inherent limitations of the algebraic mesh movement algorithm. The degradation in mesh quality leads to increased error in the flow solution and corresponding lift and drag values.

Figure 5.1: Case 1 optimized airfoil versus initial RAE 2822 airfoil

Operating Point	α	C_l	C_d	$M_{\mathbf{max}}$	$C_{\mathbf{l,max}}$
A	$-0.71°$	0.17	0.0090	-	-
B	$-0.06°$	0.28	0.0092	-	-
C	$-0.12°$	0.27	0.0101	-	-
D	$+0.93°$	0.45	0.0108	-	-
E	$-0.36°$	0.21	0.0090	-	-
F	$+0.66°$	0.36	0.0094	-	-
G	$+0.53°$	0.34	0.0104	-	-
H	$+2.10°$	0.57	0.0115	-	-
I	$-0.17°$	0.28	0.0100	1.20	-
J	$-0.85°$	0.15	0.0092	1.10	-
K	$+0.87°$	0.46	0.0136	1.30	-
L	$-0.33°$	0.25	0.0097	1.17	-
M	$+0.77°$	0.45	0.0141	1.30	-
N	$-0.39°$	0.24	0.0105	1.16	-
O	$+3.46°$	0.74	0.0383	1.40	-
P	$+0.48°$	0.40	0.0128	1.26	-
Q	$+16.50°$	-	-	-	1.43
R	$+16.50°$	-	-	-	1.40

Table 5.4: Baseline airfoil performance (RAE 2822)

all on-design points A-H are shown in Figures 5.2 and 5.3. The solutions are shock free at all eight on-design operating conditions.

Operating Point	α	C_l	C_d	$M_{\mathbf{max}}$	$C_{\mathbf{l,max}}$
A	$-0.45°$	0.17	0.0086	-	-
B	$+0.20°$	0.28	0.0088	-	-
C	$+0.14°$	0.27	0.0097	-	-
D	$+1.19°$	0.45	0.0105	-	-
E	$-0.09°$	0.21	0.0087	-	-
F	$+0.94°$	0.36	0.0092	-	-
G	$+0.82°$	0.34	0.0100	-	-
H	$+2.40°$	0.57	0.0112	-	-
I	$+0.08°$	0.28	0.0105	1.25	-
J	$-0.62°$	0.15	0.0096	1.21	-
K	$+1.25°$	0.46	0.0174	1.35	-
L	$-0.09°$	0.25	0.0100	1.23	-
M	$+1.14°$	0.45	0.0175	1.35	-
N	$-0.14°$	0.24	0.0106	1.22	-
O	$+4.72°$	0.74	0.0513	1.45	-
P	$+0.80°$	0.40	0.0150	1.33	-
Q	$+11.40°$	-	-	-	1.27
R	$+10.80°$	-	-	-	1.23

Table 5.5: On-design-first airfoil performance (Case 1)

5.2.1 Off-design points

Figures 5.4 and 5.5 show the evolution of the constraint values for off-design points I-P and Q-R, respectively, throughout the optimization procedure. Figure 5.6 shows corresponding off-design weights. At the beginning of the main optimization procedure (after the start-up on-design-first optimization but before the first weight update cycle), the off-design aerodynamic constraints are violated at points O, Q, and R, while the remaining off-design aerodynamic constraints are satisfied. Since some off-design aerodynamic

Operating Point	α	C_l	C_d	$M_{\mathbf{max}}$	$C_{\mathbf{l,max}}$
A	$-1.61°$	0.17	0.0092	-	-
B	$-0.97°$	0.28	0.0093	-	-
C	$-1.02°$	0.27	0.0102	-	-
D	$+0.02°$	0.45	0.0107	-	-
E	$-1.36°$	0.21	0.0092	-	-
F	$-0.34°$	0.36	0.0095	-	-
G	$-0.46°$	0.34	0.0104	-	-
H	$+1.11°$	0.57	0.0113	-	-
I	$-1.02°$	0.28	0.0106	1.21	-
J	$-1.66°$	0.15	0.0120	1.32	-
K	$-0.04°$	0.46	0.0129	1.28	-
L	$-1.17°$	0.25	0.0107	1.24	-
M	$-0.09°$	0.45	0.0135	1.28	-
N	$-1.21°$	0.24	0.0115	1.25	-
O	$+1.46°$	0.74	0.0201	1.35	-
P	$-0.37°$	0.40	0.0125	1.25	-
Q	$+14.64°$	-	-	-	1.63
R	$+14.47°$	-	-	-	1.63

Table 5.6: Airfoil performance after 33 weight update cycles (Case 1)

constraints are not satisfied, we must proceed with the weight update cycles, which will result in degradation in on-design performance. The off-design weights begin at their initial reference values of unity. Within the first several weight update cycles, two distinct categories of off-design points emerge from these plots:

1. Active off-design points

2. Redundant off-design points

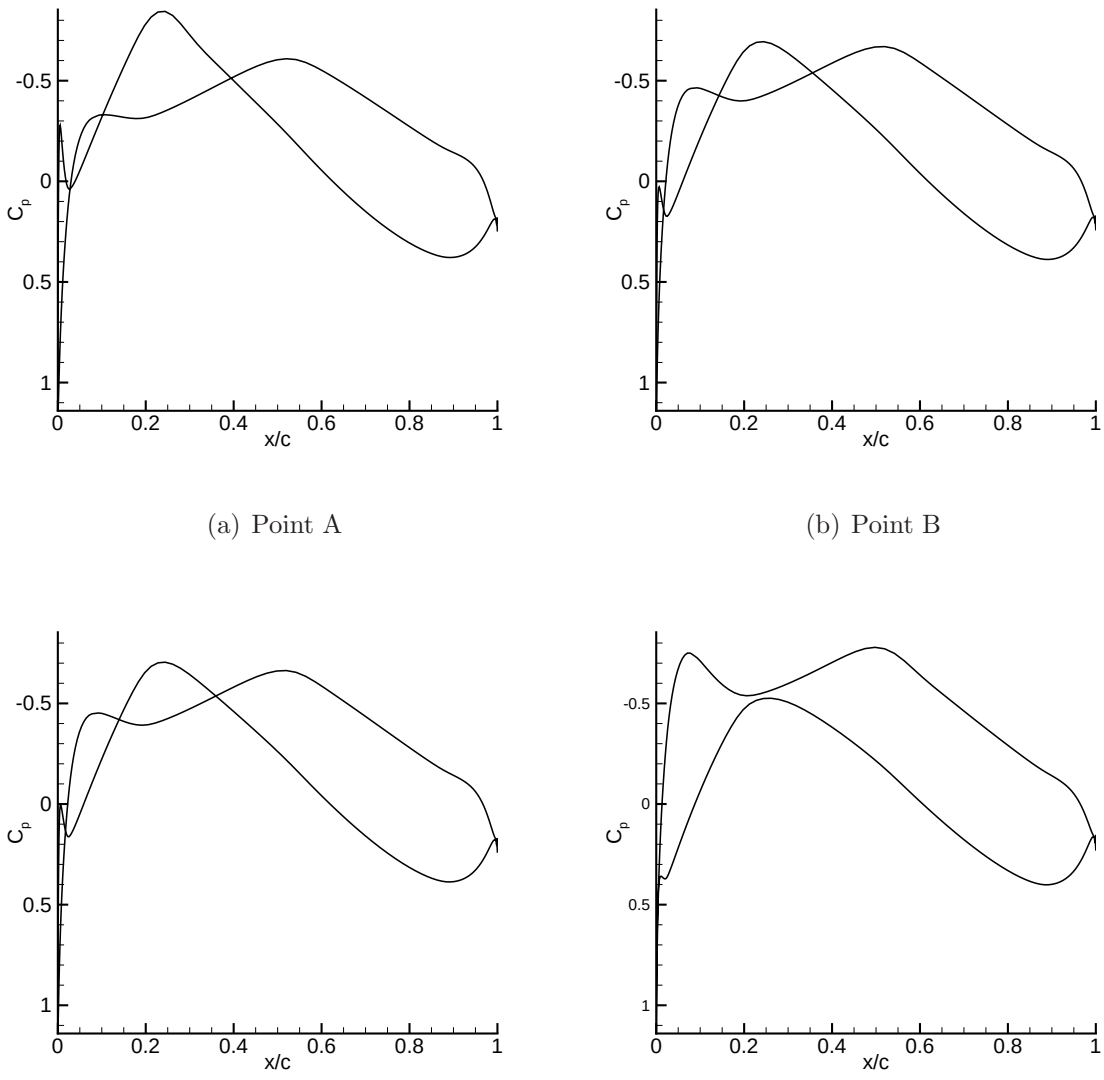

(a) Point A

(b) Point B

(c) Point C

(d) Point D

Figure 5.2: Surface pressure coefficient distributions for operating points A-D (Case 1)

Points O, Q, and R can be considered active. These points require non-zero weightings to prevent violation of their target aerodynamic constraint values. It is clear from Figure 5.6 that the off-design constraint at point O is the most difficult to satisfy, as illustrated by its high weight compared to the other active points Q, and R. Points I, J, K, L, M, N, and P can be considered redundant. These points will have their aerodynamic constraints satisfied regardless of the weight applied to them. Redundant points have

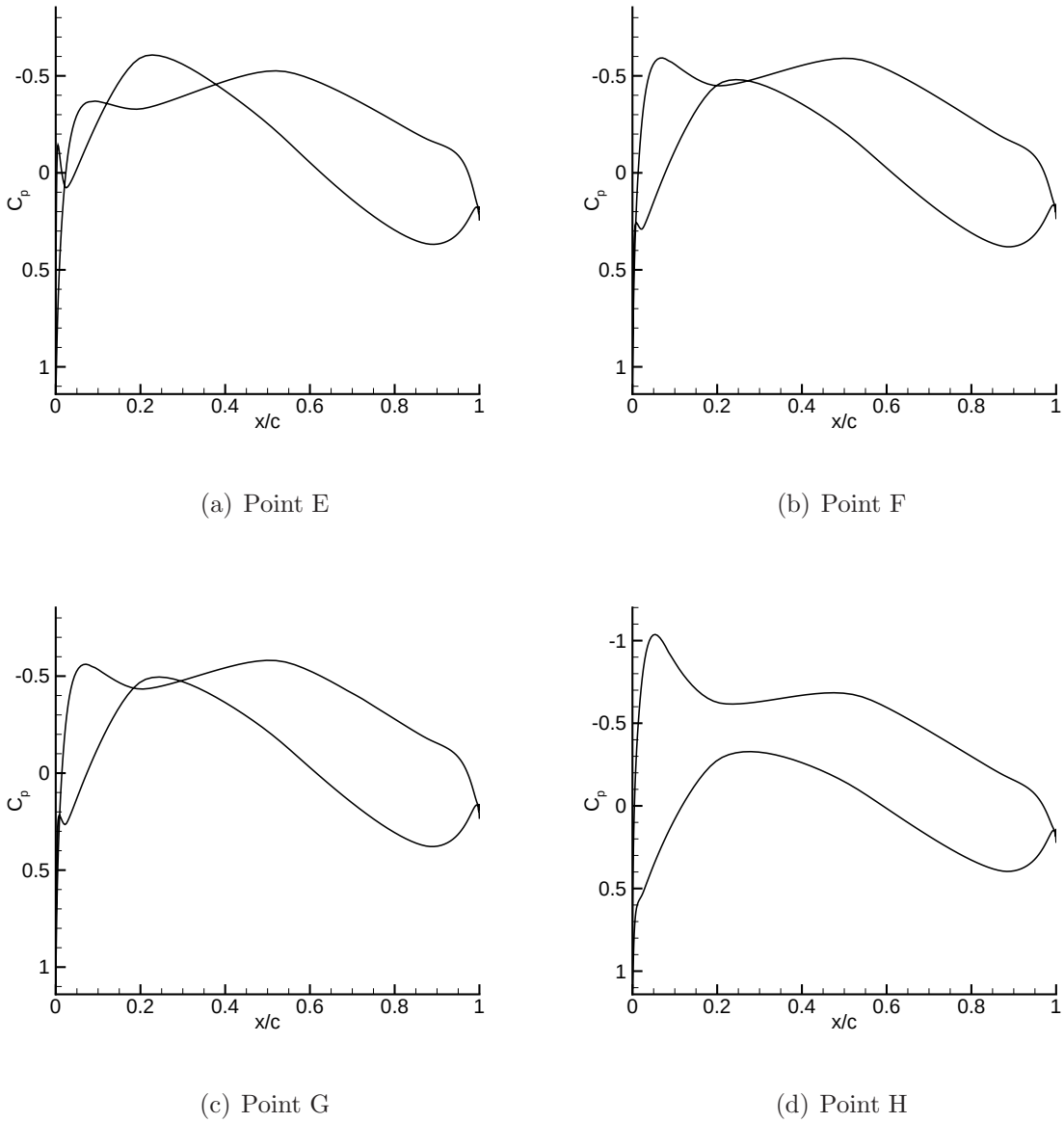

(a) Point E

(b) Point F

(c) Point G

(d) Point H

Figure 5.3: Surface pressure coefficient distributions for operating points E-H (Case 1)

their aerodynamic constraints satisfied by virtue of their proximity to active points with similar operating conditions. The weight update strategy recognizes this property of the redundant off-design points and accordingly reduces their weights to zero, as shown in Figure 5.6.

The behaviour of the active off-design points is characterized by an initial period of growth followed by asymptotic convergence of their aerodynamic constraints to their re-

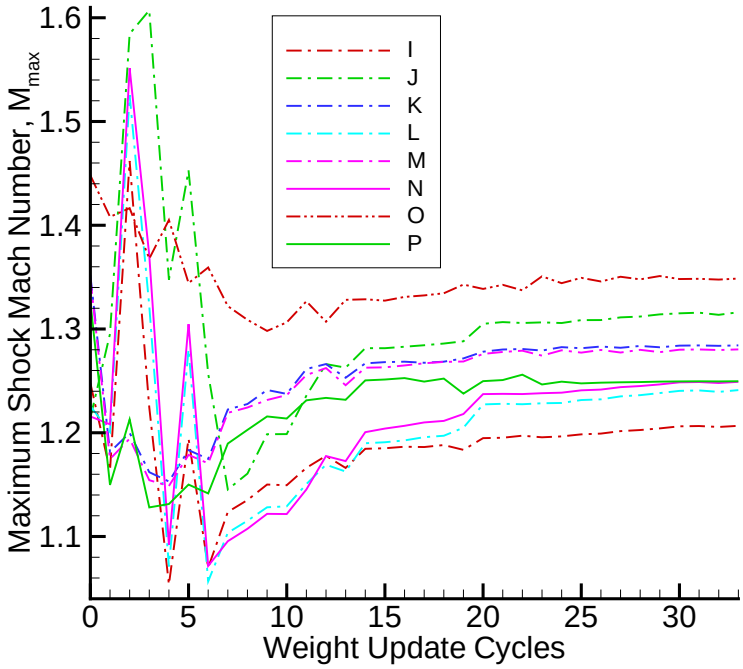

Figure 5.4: Evolution of off-design constraint values I - P

spective target values with corresponding constant weight values. The redundant points attain constant over-satisfied aerodynamic constraint values with corresponding weightings of zero. This behaviour is observed in Figures 5.4, 5.5, and 5.6.

It is likely that point Q is also redundant. Throughout the optimization procedure, the off-design constraint value at point Q, $C_{\mathrm{l,max}}$, follows slightly above the $C_{\mathrm{l,max}}$ constraint value at point R, as shown in Figure 5.5. It appears that as long as the $C_{\mathrm{l,max}}$ constraint at point R is satisfied, the $C_{\mathrm{l,max}}$ constraint at point Q will also be satisfied with a slightly higher value. The claim of redundancy of point Q can be further justified by noting that its weight is slowly approaching zero while the weight on point R remains constant during the last 10 weight update cycles. It is reasonable to assume that if the optimization were allowed to continue beyond 33 weight update cycles, the weight for point Q would eventually reach zero.

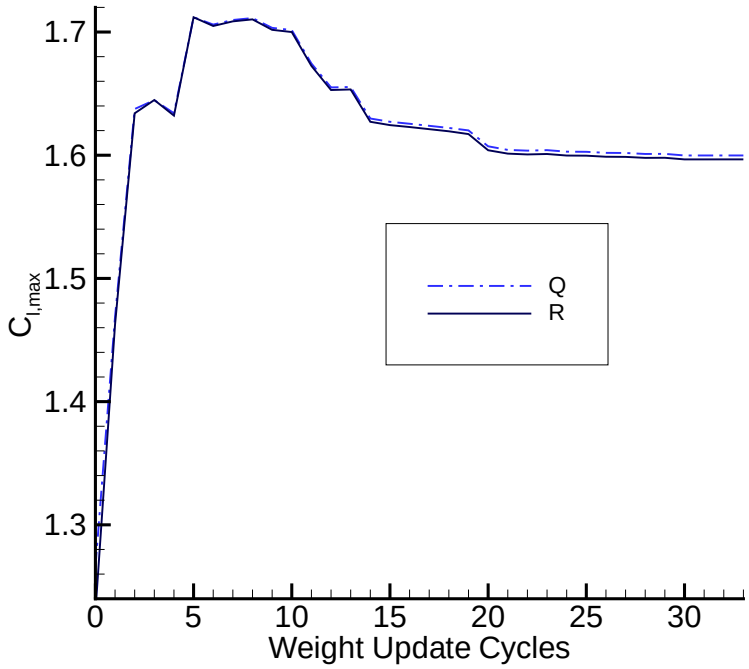

Figure 5.5: Evolution of off-design aerodynamic constraint values Q and R

5.2.2 On-design points

Since the on-design optimization weights are held constant throughout the optimization procedure, the on-design performance is evolving through the course of the optimization solely due to the shift of emphasis characterized by the relative change in the off-design weights. Figure 5.7 shows the evolution of the drag coefficients for the eight on-design points. In the first 7 weight update cycles, significant on-design performance fluctuation is clearly observable. With the introduction of the off-design points, the on-design drag values immediately begin to rise. Figure 5.8 shows the sum of the on-design drag coefficients superimposed against the sum of the off-design weights. It illustrates the relationship between on-design performance and off-design weights.

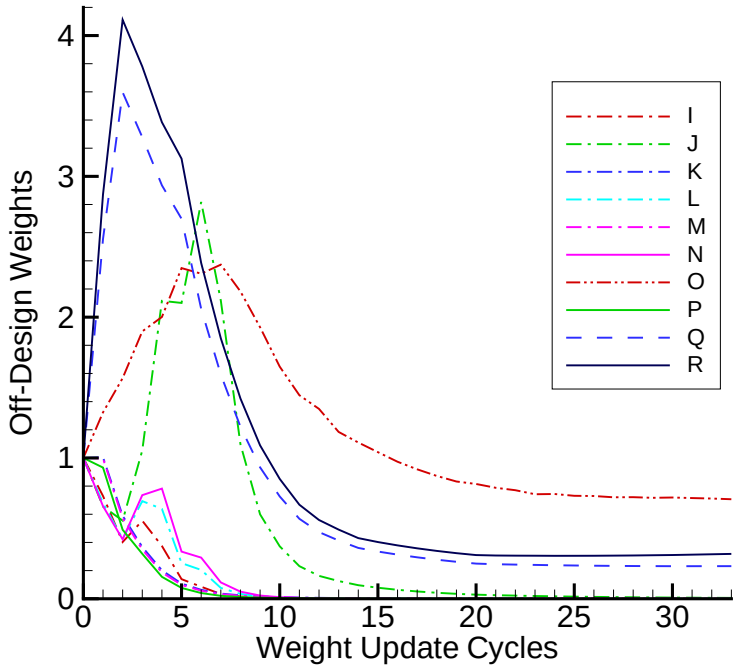

Figure 5.6: Evolution of off-design weights

5.3 Case 2 - Alternate Initial Airfoil

The initial geometry used for the optimization in this case is the NACA 0012 airfoil. The full set of 18 design points, A-R, described in Table 4.1 are used.

The results shown were obtained after 36 weight update cycles. A comparison of the optimized airfoil obtained in Case 2 versus the optimized airfoil obtained in Case 1 is shown in Figure 5.9. The initial NACA 0012 airfoil is also included in Figure 5.9 for reference. Table 5.7 shows a comparison of the performance values for the final optimized airfoil for Case 2 versus the baseline NACA 0012 airfoil performance values. The slight difference in optimized airfoil geometries can be attributed to the fixed leading edges for the airfoils in each case. Another contributing factor is the differences in the design spaces in each case resulting from the application of the mesh movement algorithm starting from two different initial airfoil geometries. A comparison of the final

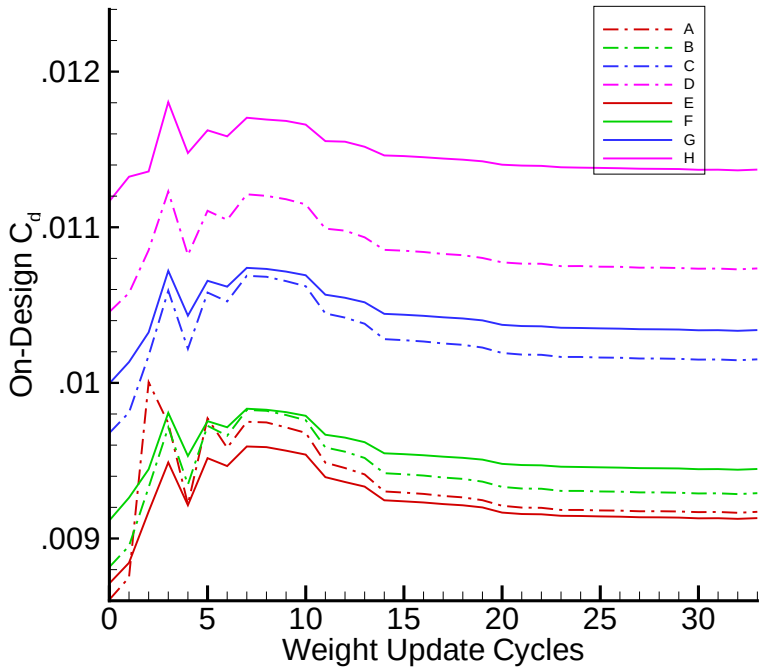

Figure 5.7: Evolution of on-design performance

off-design weights for both cases is shown in Table 5.8. The weight for off-design point O is significantly different in both cases while the weights at points Q-R are similar. The remaining redundant points are in agreement with all weights equal to zero for both cases. Given enough weight update cycles, the off-design weight for point O for Case 2 may become closer to the value obtained in Case 1, although some difference in the final point O weight for both cases should be expected because of the fixed leading edges. The substantial improvement in performance for the final optimized airfoil compared to the baseline NACA 0012 airfoil performance indicates that the NACA 0012 airfoil is poorly suited to this particular design problem. In contrast, the RAE 2822 airfoil used in Case 1 is a more appropriate first guess as a solution to this design problem in terms of initial on-design performance and violation of off-design constraints. These results show that the final airfoil geometry and performance values for Case 2 are very similar to results obtained for Case 1. This is significant because it confirms that the automated weight

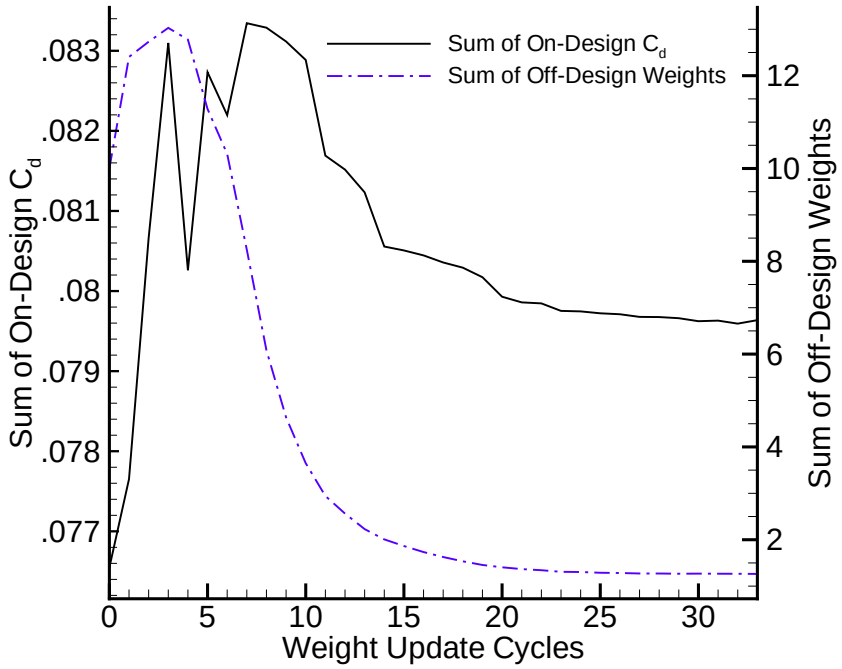

Figure 5.8: Sum of on-design performance values versus sum of off-design weights

update procedure will produce the same final optimized results independent of the initial geometry.

Figure 5.9: Case 2 optimized airfoil versus Case 1 optimized airfoil

5.4 Case 3 - Reduced Set of Off-Design Points

The initial geometry used for the optimization in this case is the NACA 0012 airfoil. A reduced set of design points is used for this case. On-design points A-H are included, but only off-design points O and R are included for a total of 10 design points. Points O and R are the only off-design points included because the results from Case 1 revealed that

Op	NACA 0012					Case 2				
Point	α	C_l	C_d	$M_{\max}$	$C_{l,\max}$	α	C_l	C_d	$M_{\max}$	$C_{l,\max}$
A	$+1.01°$	0.17	0.0092	-	-	$-1.59°$	0.17	0.0092	-	-
B	$+1.67°$	0.28	0.0105	-	-	$-0.95°$	0.28	0.0093	-	-
C	$+1.61°$	0.27	0.0111	-	-	$-1.00°$	0.27	0.0102	-	-
D	$+2.82°$	0.45	0.0188	-	-	$+0.05°$	0.45	0.0107	-	-
E	$+1.45°$	0.21	0.0093	-	-	$-1.32°$	0.21	0.0092	-	-
F	$+2.48°$	0.36	0.0100	-	-	$-0.30°$	0.36	0.0094	-	-
G	$+2.35°$	0.34	0.0108	-	-	$-0.42°$	0.34	0.0104	-	-
H	$+3.95°$	0.57	0.0136	-	-	$+1.15°$	0.57	0.0114	-	-
I	$+1.57°$	0.28	0.0160	1.34	-	$-0.99°$	0.28	0.0108	1.24	-
J	$+0.81°$	0.15	0.0110	1.27	-	$-1.67°$	0.15	0.0100	1.22	-
K	$+3.06°$	0.46	0.0337	1.47	-	$-0.04°$	0.46	0.0143	1.31	-
L	$+1.38°$	0.25	0.0146	1.32	-	$-1.15°$	0.25	0.0105	1.22	-
M	$+2.92°$	0.45	0.0326	1.46	-	$-0.09°$	0.45	0.0149	1.29	-
N	$+1.33°$	0.24	0.0149	1.32	-	$-1.21°$	0.24	0.0112	1.21	-
O	$+15.50°$	0.74	0.2545	1.68	-	$+1.46°$	0.74	0.0207	1.33	-
P	$+2.42°$	0.40	0.0261	1.42	-	$-0.37°$	0.40	0.0137	1.29	-
Q	$+15.00°$	-	-	-	1.45	$+14.61°$	-	-	-	1.64
R	$+15.00°$	-	-	-	1.44	$+14.39°$	-	-	-	1.64

Table 5.7: Case 2 optimized airfoil performance versus baseline NACA 0012 airfoil performance

the other off-design points are redundant.

Table 5.9 shows the performance values for the optimized airfoil obtained after 33 weight update cycles and a comparison of the optimized airfoil geometries from Case 3 versus Case 2 are shown in Figure 5.10. These results show that the final airfoil geometry and performance values for Case 3 are very similar to results obtained for Case 2. In

Operating Point	Case 1 Off-Design Weight	Case 2 Off-Design Weight
I	0.00	0.00
J	0.00	0.00
K	0.00	0.00
L	0.00	0.00
M	0.00	0.00
N	0.00	0.00
O	0.71	3.71
P	0.00	0.00
Q	0.23	0.26
R	0.32	0.54

Table 5.8: Comparison of final off-design weights for Case 1 and Case 2

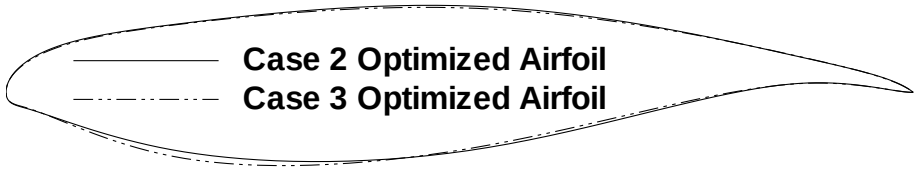

Figure 5.10: Case 3 optimized airfoil versus Case 2 optimized airfoil

practice, the knowledge regarding the redundancy of the off-design points would not be available prior to running the optimization. However it is instructive to show that the same optimized results are obtained with significantly less computational effort. Both cases required a similar number of design iterations and weight update cycles, but only 10 flow solves and adjoint calculations per design iteration were required for this case compared to 18 for Case 2. A logical extension of this work would be to investigate methods to predict redundancy of off-design points, although an experienced designer may be able to do so successfully.

Operating Point	α	C_l	C_d	$M_{\mathbf{max}}$	$C_{\mathbf{l,max}}$
A	$-1.55°$	0.17	0.0092	-	-
B	$-0.91°$	0.28	0.0093	-	-
C	$-0.96°$	0.27	0.0102	-	-
D	$+0.09°$	0.45	0.0107	-	-
E	$-1.29°$	0.21	0.0092	-	-
F	$-0.27°$	0.36	0.0094	-	-
G	$-0.39°$	0.34	0.0104	-	-
H	$+1.18°$	0.57	0.0113	-	-
I	$-0.95°$	0.28	0.0108	1.22	-
J	$-1.60°$	0.15	0.0123	1.33	-
K	$-0.03°$	0.46	0.0130	1.28	-
L	$-1.10°$	0.25	0.0108	1.25	-
M	$-0.02°$	0.45	0.0136	1.28	-
N	$-1.14°$	0.24	0.0117	1.26	-
O	$+1.51°$	0.74	0.0198	1.34	-
P	$-0.30°$	0.40	0.0125	1.25	-
Q	$+14.61°$	-	-	-	1.63
R	$+14.56°$	-	-	-	1.62

Table 5.9: Case 3 optimized airfoil performance

5.5 Case 4 - Full Set of Off-Design Points Using SNOPT

Case 4 repeats Case 1 but using the constrained optimization method instead of the off-design weight update method. The results for Case 4 were obtained after 44 SNOPT major iterations. The optimized solution satisfies the first-order optimality conditions for the constrained optimization problem. On-design performance has been optimized while

Operating Point	α	C_l	C_d	$M_{\mathbf{max}}$	$M_{\mathbf{ks}}$	$C_{\mathbf{l,max}}$
A	$-1.79°$	0.17	0.0092	-	-	-
B	$-1.16°$	0.28	0.0093	-	-	-
C	$-1.21°$	0.27	0.0102	-	-	-
D	$-0.17°$	0.45	0.0108	-	-	-
E	$-1.54°$	0.21	0.0092	-	-	-
F	$-0.53°$	0.36	0.0095	-	-	-
G	$-0.65°$	0.34	0.0104	-	-	-
H	$+0.90°$	0.57	0.0114	-	-	-
I	$-1.19°$	0.28	0.0108	1.23	1.38	-
J	$-1.85°$	0.15	0.0103	1.32	1.39	-
K	$-0.16°$	0.46	0.0144	1.31	1.44	-
L	$-1.35°$	0.25	0.0105	1.22	1.37	-
M	$-0.21°$	0.45	0.0149	1.31	1.44	-
N	$-1.40°$	0.24	0.0112	1.21	1.36	-
O	$+1.44°$	0.74	0.0219	1.35	1.50	-
P	$-0.51°$	0.40	0.0137	1.28	1.42	-
Q	$+14.35°$	-	-	-	-	1.63
R	$+14.35°$	-	-	-	-	1.63

Table 5.10: Case 4 optimized airfoil performance

all off-design constraints have been satisfied. As with Case 1, the performance results shown in Table 5.10 were obtained from regenerated meshes with the same properties as the original mesh for greater accuracy. It is important to note that at the final converged solution (before mesh regeneration) the only active off-design constraints were at points O and R whose constraint values were $M_{\text{ks}} = 1.500$ and $C_{\text{l,max}} = 1.600$, respectively. This observation supports the conclusions from Cases 1 and 3 regarding off-design constraint activity. Table 5.11 shows a comparison of the the off-design weights, ω^*, at the final

Figure 5.11: Case 4 - Optimized airfoil after 44 SNOPT major iterations

solution of Case 1, and the dual variables[3], π^*, corresponding to the off-design constraints at the final solution of Case 4. It can be seen that the KKT complementarity condition given by equation 4.13 is satisfied since the dual variables are zero at all inactive off-design constraints. The difference in sign of the dual variables at points O and R is due to the fact that the constraint at point O is bounded from above and the constraint at point R is bounded from below. A comparison of the performance results shown in Table 5.10 versus the performance results for Case 1 shown in Table 5.6 reveals that the on-design performance is very similar in both cases. However, there are differences in the off-design performance values. Figure 5.11 shows that the optimized airfoil geometries for Cases 1 and 4 are somewhat different. Further investigation is required to fully explain why two somewhat different solutions were obtained for the same optimization problem. Convergence of SNOPT is achieved with substantially less computational effort than that required using the the off-design weight update method given that the final solution of Case 4 was achieved in 501 minutes compared to approximately 6000 minutes for Case 1.

[3]In SNOPT, the dual variables are analogous to the Lagrange multipliers in a constrained optimization problem.

Operating Point	**Case 1 Off-Design Weights ω^***	**Case 4 Dual Variables π^***
I	0.00	0.00
J	0.00	0.00
K	0.00	0.00
L	0.00	0.00
M	0.00	0.00
N	0.00	0.00
O	0.71	-0.34
P	0.00	0.00
Q	0.23	0.00
R	0.32	0.18

Table 5.11: Final off-design weights for Case 1 versus final dual variables for Case 4

Chapter 6

Conclusions

Two methods for solving practical aerodynamic design problems with competing design objectives and aerodynamic constraints using multipoint optimization have been presented. Both methods address issues that arise in practical multipoint optimization due to the co-existence of on-design and off-design points. The application of the off-design weight update method to an eighteen-point airfoil optimization demonstrates that it is able to adjust off-design weights iteratively based on the evolution of aerodynamic performance so as to satisfy off-design aerodynamic constraints while minimizing the penalty in on-design performance. The method allows designers to identify redundant and critical operating points. Furthermore, this technique is capable of preventing the off-design constraints from being over-satisfied in order to minimize their negative influence on the on-design performance. The resulting airfoil for the baseline case satisfies all off-design aerodynamic constraints and has maintained overall on-design performance compared to the RAE 2822 airfoil. The main features of the off-design weight update method summarized above are described in detail in Case 1. Moreover, virtually the same optimized airfoil can be obtained starting from the NACA 0012 airfoil as shown in Case 2. An additional optimization executed using the weight update procedure with a reduced set of off-design points confirms that the same optimized airfoil can be obtained with sig-

nificantly less computational effort if redundant off-design constraints can be identified prior to performing the optimization. These results were demonstrated in Case 3.

The second method using the constrained optimization algorithm SNOPT is capable of producing the same results as the off-design weight update method but with significantly less computational effort as shown in Case 4. A drawback to the SNOPT method is the trial and error procedure required to obtain suitable values for the parameters ρ and M_{ks} associated with the KS function needed to achieve satisfaction of the M_{max} constraints. To solve a practical aerodynamic design problem using the SNOPT method, 3 or 4 trials using various combinations of ρ and M_{ks} may be required to achieve satisfaction of the M_{max} constraints. Even when the trial and error procedure associated with the SNOPT method is taken into consideration, it is still less costly in terms of time compared to the off-design weight update procedure given that it can obtain a solution (to 1 trial) more than 5 times as quickly. Although there remain some unanswered questions associated with the SNOPT method, the potential for large time savings makes a compelling argument to pursue this method further.

6.1 Future Work

6.1.1 Representative sampling of flow field Mach numbers to reduce *KS* function constraints

Generally speaking, as the number of constraints handled by the KS function decreases, its conservative estimate of the maximum constraint value becomes closer to the actual maximum constraint value. This property may be exploited by investigating strategies to reduce the number of constraints, $g(X)$, handled by the KS function, thus reducing the guesswork associated with the assignment of ρ and M_{ks}^{*} parameters. An example of such a strategy is to specify a localized region of nodes where M_{max} is expected to occur

instead of considering the Mach numbers at all nodes in the flow field as is currently being done.

6.1.2 Adaptive *KS* approach

Another option to reduce the guesswork associated with the assignment of ρ and M^*_{ks} parameters in the SNOPT method may be to use the adaptive KS approach developed by Poon and Martins [16]. Their approach increases the value of ρ above a nominal value at design iterations where the conservative estimate of M_{max}, given by M_{ks}, exceeds a user-defined tolerance. By increasing the value of ρ at such locations in the design space, the value of M_{ks} approximates M_{max} more accurately. This would allow the upper bound on the maximum Mach number constraint function, M^*_{ks}, used by SNOPT to be set equal to the actual upper bound, M^*_{max}. Using the adaptive KS approach, it is expected that the value of M_{max} for all active constraints at the converged solution would be within a user-defined tolerance of M^*_{ks}.

6.1.3 Design under uncertainty

The concept of design under uncertainty recognizes that various uncertainties associated with certain parameters involved in the optimization procedure can lead to significant uncertainty in the optimal solution. For example, in Case 1, at the optimized solution, the active M_{max} constraint at point O is satisfied for an angle of attack $\alpha = +1.46°$. In the event that an airplane experiences this dive operating condition, the pilot cannot be expected to hold the airplane at the exact angle of attack prescribed by the optimal solution. A more realistic expectation is that the angle attack is allowed some acceptable range of variance about the ideal value, and within this range, the M_{max} constraint at point O remains satisfied. To achieve this goal, the optimization must consider the uncertainty surrounding the angle of attack parameter. In order to further increase the usefulness of the methods presented, it would be beneficial to incorporate a methodology

for dealing with this type of uncertainty. For a comprehensive survey of the state-of-the-art in uncertainty-based design of aerospace vehicles, see [23]. Specific applications within the context of aerodynamic shape optimization can be found in [21, 14, 7].

6.1.4 Linearize pressure switch used in artificial dissipation calculation

The use of second-order artificial dissipation is necessary to maintain flow solution stability for strongly non-linear cases, such as those with strong shocks [17]. The RAE 2822 and NACA 0012 airfoils used in the cases of Chapter 5 were chosen specifically because the strength of shocks produced at the operating conditions considered were sufficiently weak to allow the cases to be run without second-order artificial dissipation. However, it is very difficult to obtain a converged flow solution at point O for the NACA 0015 airfoil, for example, without using second-order artificial dissipation. Currently, using second-order artificial dissipation for optimization cases is not recommended because it has been shown by Nemec [10] to reduce the accuracy of the adjoint gradient calculation. The source of this inaccuracy can be attributed to the pressure switch that is used in the calculation of the second-order artificial dissipation term. The pressure switch values are incorrectly treated as constants during the differentiation of the residual equations required for the adjoint gradient calculation. A hand coded analytic derivative of the pressure switch would address this issue and restore accuracy to the adjoint gradient calculation. It should be noted that the pressure switch is not actually differentiable due to the presence of a maximum function in its definition, but a reasonable approximation of its derivative is achievable. An accurate gradient with second-order artificial dissipation would allow for an expanded range of practical aerodynamic design problems to be investigated.

6.1.5 Automated design point generation

The design point definitions given for the 18-point optimization described in Section 4.1 were taken as a representative sample of the continuous range of operating conditions for an airplane. It is assumed that by optimizing at these points, good performance will be achieved everywhere. In some cases, this may not be true. To avoid poor performance at operating conditions away from the design points, an automated procedure to check performance at intermediate operating conditions between design points may be employed. If an area of poor performance is identified, a design point could be added at this location to improve performance.

6.1.6 Effect of the number of design variables on optimization

Considering that the computational cost of an airfoil optimization increases as the number of design variables increases, it would be worthwhile to investigate the effect of the number of design variables on the results of an optimization. More specifically, how does the final optimized airfoil shape and performance compare for differing numbers of design variables? For a given optimization problem, is there a practical limit on the number of design variables beyond which the differences in shape and performance are negligible?

As part of this study, it would be interesting to investigate Drela's theorem [4] regarding the phenomenon of point optimization[1]. This theorem relates the number of design variables to the number of design points. It states that a multipoint optimization needs at least $m + 1$ design points to avoid point optimization where m is the number of free design variables.

[1]Point optimization refers to optimal performance only in the local vicinity of a design point and poor performance at locations away from the design point.

6.1.7 Effect of mesh density on optimization

The computational cost of optimization is also related to the density of nodes in the mesh used by the flow solver. As the number of nodes increases, the time taken to obtain a flow solution increases. With large numbers of design points in a practical aerodynamic design problem, the cost of calculating flow solutions is significant. It is known that the predicted performance characteristics of an airfoil become more accurate as the mesh density increases. However, the question we seek to answer is *how will the geometries of optimized airfoils obtained using different mesh densities compare?* Ideally, the same shape can be obtained using a range of different mesh densities. If this is the case, then meshes at the low end of the density range should be favoured for optimization problems to improve computational efficiency. A problem with coarse mesh optimization has been identified regarding specifying an appropriate $C_{\mathrm{l,max}}$ target. From experience, it is known that the value of $C_{\mathrm{l,max}}$ will increase significantly as the mesh density increases. This makes it difficult to specify an appropriate $C_{\mathrm{l,max}}$ target for coarse mesh optimization to achieve the desired grid-converged value of $C_{\mathrm{l,max}}$.

6.1.8 Pareto front generation

Practical aerodynamic design problems involve competing objectives. Pareto fronts are a useful tool for a designer to gain an understanding of the tradeoffs between competing objectives by means of a graphical representation. A Pareto front defines a family of optimal solutions obtained by varying the weights associated with each of the design objectives. Nemec [10] provides a good example of a multi-objective airfoil design problem with a corresponding set of Pareto-optimal solutions. A framework for defining objectives of interest may be employed to automatically generate a Pareto-optimal set of solutions. The difficulty with a large multipoint optimization lies in determining logical groupings of design objectives to compare using Pareto fronts. Examples of such groupings are a

comparison of cruise conditions to long-range cruise conditions or on-design performance versus off-design constraint targets.

6.1.9 Extension of methods to three-dimensional optimization problems

The two methods for solving practical aerodynamic design problems have been demonstrated on two-dimensional airfoils. Although important insights can be gained from two-dimensional analysis and optimization, three dimensions are required for a more accurate portrayal of the physical reality experienced by airplanes. Given a reliable and robust set of three-dimensional design evaluation tools, an extension of these methods to three-dimensional optimization problems is reasonably straightforward. The main difference is that the number of critical design parameters increases by an order of magnitude, such as design variables, mesh size and geometric constraints, to name a few. The computational efficiency of the methods becomes significantly more important given the size of the problems in terms of parallel processing, memory, and time requirements.

References

[1] W. K. Anderson and D. L. Bonhaus. Aerodynamic Design On Unstructured Grids for Turbulent Flows. Technical Report TM-112867, NASA, 1997.

[2] L. K. Billing. On The Development of An Improved Lift-Constrained Aerodynamic Optimization Algorithm. Master's thesis, University of Toronto, 2006.

[3] S. E. Cliff, J. J. Reuther, D. A. Saunders, and R. M. Hicks. Single-Point and Multipoint Aerodynamic Optimization of High Speed Civil Transport. *Journal of Aircraft*, 38(6), November-December 2001.

[4] M. Drela. *Frontiers of Computational Fluid Dynamics*, chapter Pros and Cons of Airfoil Optimization, pages 363–381. World Scientific, 1998.

[5] B. Epstein, A. Jameson, S. Peigin, D. Roman, N. Harrison, and J. Vassberg. Comparative Study of 3D Wing Drag Minimization by Different Optimization Techniques. *Journal of Aircraft*, 46(2), March-April 2009.

[6] P. E. Gill, W. Murray, and M. A. Saunders. SNOPT: An SQP Algorithm for Large-Scale Constrained Optimization. *SIAM Review*, 47(1):99–131, February 2005.

[7] L. Huyse, S. L. Padula, R. M. Lewis, and W. Li. Probabilistic Approach to Free-Form Airfoil Shape Optimization Under Uncertainty. *AIAA Journal*, 40(9), September 2002.

[8] W. Li, L. Huyse, and S. Padula. Robust Airfoil Optimization to Achieve Consistent Drag Reduction Over a Mach Range. ICASE 2001-22, NASA, August 2001.

[9] J. R. R. A. Martins, J. J. Alonso, and J. J. Reuther. High-Fidelity Aerostructural Design Optimization of a Supersonic Business Jet. *Journal of Aircraft*, 41(3):523–530, 2004.

[10] M. Nemec. *Optimal Shape Design of Aerodynamic Configurations: A Newton-Krylov Approach*. PhD thesis, The University of Toronto, 2003.

[11] M. Nemec and D. W. Zingg. Newton-Krylov Algorithm for Aerodynamic Design Using the Navier-Stokes Equations. *AIAA Journal*, 40(6):1146–1154, June 2002.

[12] M. Nemec, D. W. Zingg, and T. H. Pulliam. Multipoint and Multi-Objective Aerodynamic Shape Optimization. *AIAA Journal*, 42(6):1057–1065, June 2004.

[13] J. Nocedal and S. Wright. *Numerical Optimization*. Springer, 2nd edition, 2006.

[14] S. Padula. Aerospace Applications of Optimization Under Uncertainty. *Optimization and Engineering*, 7:317–328, 2006.

[15] O. Pironneau. On Optimum Design in Fluid Mechanics. *Journal of Fluid Mechanics*, 64(1):97–110, 1974.

[16] N. M. K. Poon and J. R. R. A. Martins. An Adaptive Approach to Constraint Aggregation Using Adjoint Sensitivity Analysis. *Structural Multidisciplinary Optimization*, 34:61–73, 2006.

[17] T. H. Pulliam and D. W. Zingg. *Foundations of Computational Fluid Dynamics*, chapter 4, page 35. (unpublished), August 2007.

[18] D. F. Shanno and K. H. Phua. Algorithm 500, Minimization of Unconstrained Multivariate Functions. *ACM Transactions on Mathematical Software*, 2(1):87–94, 1976.

[19] P. R. Spalart and S. R. Allmaras. A One-Equation Turbulence Model For Aerodynamic Flows. *AIAA Journal*, (92-0439), January 1992.

[20] M. Stettner and D. P. Schrage. An Approach to Tiltrotor Wing Aeroservoelastic Optimization. *AIAA/USAF/NASA/OAI*, 1992. 4th Symposium on Multidisciplinary Analysis and Optimization, Cleveland, Ohio.

[21] L. Z. Tang, J. Periaux, and J. A. Desideri. Multi Criteria Robust Design Using Adjoint Methods and Game Strategies For Solving Drag Optimization Problems With Uncertainties. In *West-East High Speed Flow Field Conference Proceedings*, Beijing, October 2005.

[22] G. A. Wrenn. An Indirect Method for Numerical Optimization Using the Kreisselmeier-Steinhauser Function. Technical Report CR-4220, NASA, 1989.

[23] T. Zang, M. Hemsch, M. Hillburger, S. Kenny, J. Luckring, P. Maghami, S. Padula, and W. Stroud. Needs And Opportunities for Uncertainty-Based Multidisciplinary Design Methods for Aerospace Vehicles. Technical Report TM-2002-211462, NASA, July 2002.

[24] B. Zhou. UTIAS 2007 Summer Project Report. unpublished, August 2007.

[25] D. W. Zingg and L. Billing. Toward Practical Aerodynamic Design Through Numerical Optimization. *AIAA Journal*, 2007.

[26] D. W. Zingg and S. Elias. Aerodynamic Optimization Under a Range of Operating Conditions. *AIAA Journal*, 44(11):2787–2792, November 2006.

Appendix A

Input Files

A.1 Case 1

```
MP-OPT
  18
WEIGHT OFF_DES FSMACH CL_TAR WFL CD_TAR RE DVALFA ALPHA OBJ_FUNC CLALPHA CLALPHA2 CLOPT

 1.0   FALSE   0.72  0.17  1.0  0.01   27.32e6  FALSE  0.04 8  TRUE  TRUE  TRUE
 1.0   FALSE   0.72  0.28  1.0  0.01   27.32e6  FALSE  0.63 8  TRUE  TRUE  TRUE
 1.0   FALSE   0.72  0.27  1.0  0.01   18.57e6  FALSE  0.59 8  TRUE  TRUE  TRUE
 1.0   FALSE   0.72  0.45  1.0  0.01   18.57e6  FALSE  1.65 8  TRUE  TRUE  TRUE
 1.0   FALSE   0.64  0.21  1.0  0.01   24.22e6  FALSE  1.5  8  TRUE  TRUE  TRUE
 1.0   FALSE   0.64  0.36  1.0  0.01   24.22e6  FALSE  2.6  8  TRUE  TRUE  TRUE
 1.0   FALSE   0.64  0.34  1.0  0.01   16.46e6  FALSE  2.5  8  TRUE  TRUE  TRUE
 1.0   FALSE   0.64  0.57  1.0  0.01   16.46e6  FALSE  4.5  8  TRUE  TRUE  TRUE

 0.730   FALSE   0.76  0.28  1.0  0.01   28.88e6  FALSE  1.0  8  TRUE  TRUE  TRUE
 0.655   FALSE   0.76  0.15  1.0  0.01   28.88e6  FALSE  1.0  8  TRUE  TRUE  TRUE
 1.005   FALSE   0.76  0.46  1.0  0.01   28.88e6  FALSE  1.0  8  TRUE  TRUE  TRUE
 0.680   FALSE   0.76  0.25  1.0  0.01   28.88e6  FALSE  1.0  8  TRUE  TRUE  TRUE
 0.996   FALSE   0.76  0.45  1.0  0.01   19.62e6  FALSE  1.0  8  TRUE  TRUE  TRUE
 0.658   FALSE   0.76  0.24  1.0  0.01   19.62e6  FALSE  1.0  8  TRUE  TRUE  TRUE
 1.324   FALSE   0.76  0.74  1.0  0.01   19.62e6  FALSE  1.0  8  TRUE  TRUE  TRUE
 0.932   FALSE   0.76  0.40  1.0  0.01   19.62e6  FALSE  1.0  8  TRUE  TRUE  TRUE

 2.555  FALSE   0.16  2.00   1.0  0.01   11.8e6  TRUE   11.40 6  FALSE  FALSE  FALSE
 2.871  FALSE   0.20  2.00   1.0  0.01   15.0e6  TRUE   10.80 6  FALSE  FALSE  FALSE

&OPTIMA
   OPT_METH = 3,  OPT_ITER = 300, OPT_TOL = 1.d-5,
   OPT_RESTART = FALSE, GRADIENT = 1, CDF = TRUE, FD_ETA  = 1.d-6,
   COEF_FRZ = FALSE, IFRZ_WHAT = 3, WFACTOR = 0.1, BSTEP = 0.1,
   AUTO_RESTART = FALSE, NUM_RESTARTS = 5,GRID_HIS = TRUE,
   SOL_HIS = FALSE, OBJ_RESTART = FALSE,

   INORD = 2, IREORD = 2,
   ILU_METH = 2, LFIL = 6, PDC = 3.0,
   IM_GMRES = 85, EPS_GMRES = 1.d-8, ITER_GMRES = 500,
```

```
   NTCON=2, WFD=0.0, WTC=50.0,
   CTX     =0.95,0.99,
   CTY_TAR =0.01,0.002,

   WAC=0.0, AREAFAC=1.0

   NRTCON = 1, crtxl = 0.10d0, crtxt = 0.90d0, crtxn = 15,
   crthtar = 0.119d0
&END
&CYCLONE
   JMAX=289, KMAX=65, JTAIL1=33, JTAIL2=257,

   TRANSLO=0.01, TRANSUP=0.01,
   CLINPUT= 0.17, CLTOL=1.0d-11,
   RELAXCL=3.0,   ICLFREQ=50,   ICLSTRT=100,

   RESTART=FALSE, JACDT=1, IREAD=2, BCAIRF=TRUE, CIRCUL=FALSE,
   IORD=2, INTEG=2, CMESH=FALSE,

   IDMODEL=1,
   DIS2X   = 0.0,  DIS4X = 0.02,  DIS2Y = 0.0,  DIS4Y = 0.02,
   VLXI    = 0.25, VNXI  = 0.25,  VLETA = 0.25, VNETA = 0.25,
   LIMITER = 1,    EPZ   = 1.d-3, EPV   = 5.d0,

   PREC = 0, PRXI = 0.0, PRPHI = 1.0,

   TURBULNT = TRUE, ITMODEL = 2,    ISPBC = 1,     VISCEIG  = 1.d0,
   VISCOUS  = TRUE, VISETA  = TRUE, VISXI = FALSE, VISCROSS = FALSE,

   NCP = 1000, NQ = 1000,

   SNGVALTE   = FALSE, GRDSEQ_REST = FALSE, SV_GRDSEQ = FALSE,
   WRITERESID = FALSE, TIMING      = FALSE, WRITETURB = FASLE,
   FLBUD      = FALSE, PCHORD      = 0.32,  SKNFRC    = TRUE
&END
&PROBE
   NK_ITS = 100,   NK_ILU   = 2,  NK_LFIL  = 2, NK_PFRZ  = 1,
   NK_PDC = 6.d0, NK_IMGMR = 40, NK_ITGMR = 40
&END
&EXTRA
   grid_file_prefix = 'grid-new',
   output_file_prefix = 'rest00',
   restart_file_prefix = 'rest00'
&END
&GRAPH
   graphout = false, graph_mode = 1, interval = 0,
   num_graph= 0,
   graph_pt= 0
&END
1.E-6  | AF Convergence criteria: AF_MINR
5.E-13                          | Convergence criteria: MIN_RES
1.E-8                           | Min. res. in turb. mod. : SPMIN_RES
ISEQUAL
     1
```

```
JMXI    KMXI    IENDS    DTISEQ   DTMIS   DTOW
289     65      20000      5.0     0.0    1.d1
```

A.2 Case 2

```
MP-OPT
  18
WEIGHT OFF_DES FSMACH CL_TAR WFL CD_TAR RE DVALFA ALPHA OBJ_FUNC CLALPHA CLALPHA2 CLOPT

 1.0   FALSE   0.72  0.17  1.0  0.01   27.32e6  FALSE  0.04 8  TRUE  TRUE  TRUE
 1.0   FALSE   0.72  0.28  1.0  0.01   27.32e6  FALSE  0.63 8  TRUE  TRUE  TRUE
 1.0   FALSE   0.72  0.27  1.0  0.01   18.57e6  FALSE  0.59 8  TRUE  TRUE  TRUE
 1.0   FALSE   0.72  0.45  1.0  0.01   18.57e6  FALSE  1.65 8  TRUE  TRUE  TRUE
 1.0   FALSE   0.64  0.21  1.0  0.01   24.22e6  FALSE  1.5  8  TRUE  TRUE  TRUE
 1.0   FALSE   0.64  0.36  1.0  0.01   24.22e6  FALSE  2.6  8  TRUE  TRUE  TRUE
 1.0   FALSE   0.64  0.34  1.0  0.01   16.46e6  FALSE  2.5  8  TRUE  TRUE  TRUE
 1.0   FALSE   0.64  0.57  1.0  0.01   16.46e6  FALSE  4.5  8  TRUE  TRUE  TRUE

 0.674   FALSE   0.76  0.28  1.0  0.01   28.88e6  FALSE  1.0  8  TRUE  TRUE  TRUE
 0.626   FALSE   0.76  0.15  1.0  0.01   28.88e6  FALSE  1.0  8  TRUE  TRUE  TRUE
 0.951   FALSE   0.76  0.46  1.0  0.01   28.88e6  FALSE  1.0  8  TRUE  TRUE  TRUE
 0.623   FALSE   0.76  0.25  1.0  0.01   28.88e6  FALSE  1.0  8  TRUE  TRUE  TRUE
 0.946   FALSE   0.76  0.45  1.0  0.01   19.62e6  FALSE  1.0  8  TRUE  TRUE  TRUE
 0.601   FALSE   0.76  0.24  1.0  0.01   19.62e6  FALSE  1.0  8  TRUE  TRUE  TRUE
 1.190   FALSE   0.76  0.74  1.0  0.01   19.62e6  FALSE  1.0  8  TRUE  TRUE  TRUE
 0.906   FALSE   0.76  0.40  1.0  0.01   19.62e6  FALSE  1.0  8  TRUE  TRUE  TRUE

 1.590  FALSE   0.16  2.00   1.0  0.01   11.8e6  TRUE   14.50 6  FALSE  FALSE  FALSE
 1.710  FALSE   0.20  2.00   1.0  0.01   15.0e6  TRUE   13.50 6  FALSE  FALSE  FALSE

&OPTIMA
   OPT_METH = 3,  OPT_ITER = 300, OPT_TOL = 1.d-5,
   OPT_RESTART = FALSE, GRADIENT = 1, CDF = TRUE, FD_ETA  = 1.d-6,
   COEF_FRZ = FALSE, IFRZ_WHAT = 3, WFACTOR = 0.1, BSTEP = 0.1,
   AUTO_RESTART = FALSE, NUM_RESTARTS = 5,GRID_HIS = TRUE,
   SOL_HIS = FALSE, OBJ_RESTART = FALSE,

   INORD = 2, IREORD = 2,
   ILU_METH = 2, LFIL = 6, PDC = 3.0,
   IM_GMRES = 85, EPS_GMRES = 1.d-8, ITER_GMRES = 500,

   NTCON=2, WFD=0.0, WTC=50.0,
   CTX     =0.95,0.99,
   CTY_TAR =0.01,0.002,

   WAC=0.0, AREAFAC=1.0

   NRTCON = 1, crtxl = 0.10d0, crtxt = 0.90d0, crtxn = 15,
   crthtar = 0.119d0
&END
&CYCLONE
   JMAX=289, KMAX=65, JTAIL1=33, JTAIL2=257,

   TRANSLO=0.01, TRANSUP=0.01,
   CLINPUT= 0.17, CLTOL=1.0d-11,
   RELAXCL=3.0,   ICLFREQ=50,   ICLSTRT=100,
```

```
   RESTART=FALSE, JACDT=1, IREAD=2, BCAIRF=TRUE, CIRCUL=FALSE,
   IORD=2, INTEG=2, CMESH=FALSE,

   IDMODEL=1,
   DIS2X   = 0.0,  DIS4X = 0.02,  DIS2Y = 0.0,  DIS4Y = 0.02,
   VLXI    = 0.25, VNXI  = 0.25,  VLETA = 0.25, VNETA = 0.25,
   LIMITER = 1,    EPZ   = 1.d-3, EPV   = 5.d0,

   PREC = 0, PRXI = 0.0, PRPHI = 1.0,

   TURBULNT = TRUE, ITMODEL = 2,    ISPBC = 1,     VISCEIG  = 1.d0,
   VISCOUS  = TRUE, VISETA  = TRUE, VISXI = FALSE, VISCROSS = FALSE,

   NCP = 1000, NQ = 1000,

   SNGVALTE   = FALSE, GRDSEQ_REST = FALSE, SV_GRDSEQ = FALSE,
   WRITERESID = FALSE, TIMING      = FALSE, WRITETURB = FASLE,
   FLBUD      = FALSE, PCHORD      = 0.32,  SKNFRC    = TRUE
&END
&PROBE
   NK_ITS = 100,   NK_ILU   = 2,  NK_LFIL  = 2, NK_PFRZ  = 1,
   NK_PDC = 6.d0, NK_IMGMR = 40, NK_ITGMR = 40
&END
&EXTRA
   grid_file_prefix = 'grid-new',
   output_file_prefix = 'rest00',
   restart_file_prefix = 'rest00'
&END
&GRAPH
   graphout = false, graph_mode = 1, interval = 0,
   num_graph= 0,
   graph_pt= 0
&END
1.E-6  | AF Convergence criteria: AF_MINR
5.E-13                          | Convergence criteria: MIN_RES
1.E-8                           | Min. res. in turb. mod. : SPMIN_RES
ISEQUAL
     1
   JMXI    KMXI    IENDS    DTISEQ   DTMIS   DTOW
   289     65      20000      5.0     0.0    1.d1
```

A.3 Case 3

```
MP-OPT
  10
WEIGHT OFF_DES FSMACH CL_TAR WFL CD_TAR RE DVALFA ALPHA OBJ_FUNC CLALPHA CLALPHA2 CLOPT

 1.0   FALSE   0.72  0.17  1.0  0.01   27.32e6  FALSE  0.04 8  TRUE  TRUE  TRUE
 1.0   FALSE   0.72  0.28  1.0  0.01   27.32e6  FALSE  0.63 8  TRUE  TRUE  TRUE
 1.0   FALSE   0.72  0.27  1.0  0.01   18.57e6  FALSE  0.59 8  TRUE  TRUE  TRUE
 1.0   FALSE   0.72  0.45  1.0  0.01   18.57e6  FALSE  1.65 8  TRUE  TRUE  TRUE
 1.0   FALSE   0.64  0.21  1.0  0.01   24.22e6  FALSE  1.5  8  TRUE  TRUE  TRUE
 1.0   FALSE   0.64  0.36  1.0  0.01   24.22e6  FALSE  2.6  8  TRUE  TRUE  TRUE
 1.0   FALSE   0.64  0.34  1.0  0.01   16.46e6  FALSE  2.5  8  TRUE  TRUE  TRUE
 1.0   FALSE   0.64  0.57  1.0  0.01   16.46e6  FALSE  4.5  8  TRUE  TRUE  TRUE

 1.190   FALSE   0.76  0.74  1.0  0.01   19.62e6  FALSE  1.0  8  TRUE  TRUE  TRUE
 1.710  FALSE   0.20  2.00   1.0  0.01   15.0e6  TRUE   13.50 6  FALSE  FALSE  FALSE

&OPTIMA
   OPT_METH = 3,  OPT_ITER = 300, OPT_TOL = 1.d-5,
   OPT_RESTART = FALSE, GRADIENT = 1, CDF = TRUE, FD_ETA  = 1.d-6,
   COEF_FRZ = FALSE, IFRZ_WHAT = 3, WFACTOR = 0.1, BSTEP = 0.1,
   AUTO_RESTART = FALSE, NUM_RESTARTS = 5,GRID_HIS = TRUE,
   SOL_HIS = FALSE, OBJ_RESTART = FALSE,

   INORD = 2, IREORD = 2,
   ILU_METH = 2, LFIL = 6, PDC = 3.0,
   IM_GMRES = 85, EPS_GMRES = 1.d-8, ITER_GMRES = 500,

   NTCON=2, WFD=0.0, WTC=50.0,
   CTX     =0.95,0.99,
   CTY_TAR =0.01,0.002,

   WAC=0.0, AREAFAC=1.0

   NRTCON = 1, crtxl = 0.10d0, crtxt = 0.90d0, crtxn = 15,
   crthtar = 0.119d0
&END
&CYCLONE
   JMAX=289, KMAX=65, JTAIL1=33, JTAIL2=257,

   TRANSLO=0.01, TRANSUP=0.01,
   CLINPUT= 0.17, CLTOL=1.0d-11,
   RELAXCL=3.0,   ICLFREQ=50,   ICLSTRT=100,

   RESTART=FALSE, JACDT=1, IREAD=2, BCAIRF=TRUE, CIRCUL=FALSE,
   IORD=2, INTEG=2, CMESH=FALSE,

   IDMODEL=1,
   DIS2X   = 0.0,  DIS4X = 0.02,  DIS2Y = 0.0,  DIS4Y = 0.02,
   VLXI    = 0.25, VNXI  = 0.25,  VLETA = 0.25, VNETA = 0.25,
   LIMITER = 1,    EPZ   = 1.d-3, EPV   = 5.d0,

   PREC = 0, PRXI = 0.0, PRPHI = 1.0,
```

```
   TURBULNT = TRUE, ITMODEL = 2,    ISPBC = 1,     VISCEIG  = 1.d0,
   VISCOUS  = TRUE, VISETA  = TRUE, VISXI = FALSE, VISCROSS = FALSE,

   NCP = 1000, NQ = 1000,

   SNGVALTE   = FALSE, GRDSEQ_REST = FALSE, SV_GRDSEQ = FALSE,
   WRITERESID = FALSE, TIMING      = FALSE, WRITETURB = FASLE,
   FLBUD      = FALSE, PCHORD      = 0.32,  SKNFRC    = TRUE
&END
&PROBE
   NK_ITS = 100,   NK_ILU   = 2,  NK_LFIL  = 2, NK_PFRZ  = 1,
   NK_PDC = 6.d0, NK_IMGMR = 40, NK_ITGMR = 40
&END
&EXTRA
   grid_file_prefix = 'grid-new',
   output_file_prefix = 'rest00',
   restart_file_prefix = 'rest00'
&END
&GRAPH
   graphout = false, graph_mode = 1, interval = 0,
   num_graph= 0,
   graph_pt= 0
&END
1.E-6  | AF Convergence criteria: AF_MINR
5.E-13                          | Convergence criteria: MIN_RES
1.E-8                           | Min. res. in turb. mod. : SPMIN_RES
ISEQUAL
     1
   JMXI    KMXI    IENDS    DTISEQ   DTMIS   DTOW
   289     65      20000      5.0     0.0    1.d1
```

A.4 Case 4

```
 MP-OPT
   18
WEIGHT OFF_DES C_UPP C_LOW  FSMACH CL_TAR WFL CD_TAR RE DVALFA ALPHA OBJ_FUNC CLALPHA CLALPHA2 CLOPT

  1.0 FALSE 0.00 0.00  0.72  0.17  1.0  0.01   27.32e6  FALSE  0.04 8  TRUE  TRUE  TRUE
  1.0 FALSE 0.00 0.00  0.72  0.28  1.0  0.01   27.32e6  FALSE  0.63 8  TRUE  TRUE  TRUE
  1.0 FALSE 0.00 0.00  0.72  0.27  1.0  0.01   18.57e6  FALSE  0.59 8  TRUE  TRUE  TRUE
  1.0 FALSE 0.00 0.00  0.72  0.45  1.0  0.01   18.57e6  FALSE  1.65 8  TRUE  TRUE  TRUE
  1.0 FALSE 0.00 0.00  0.64  0.21  1.0  0.01   24.22e6  FALSE  1.5  8  TRUE  TRUE  TRUE
  1.0 FALSE 0.00 0.00  0.64  0.36  1.0  0.01   24.22e6  FALSE  2.6  8  TRUE  TRUE  TRUE
  1.0 FALSE 0.00 0.00  0.64  0.34  1.0  0.01   16.46e6  FALSE  2.5  8  TRUE  TRUE  TRUE
  1.0 FALSE 0.00 0.00  0.64  0.57  1.0  0.01   16.46e6  FALSE  4.5  8  TRUE  TRUE  TRUE

  0.0 TRUE  1.50 -1E+20 0.76  0.28  1.0  0.01   28.88e6  FALSE  1.0  12  TRUE  TRUE  TRUE
  0.0 TRUE  1.50 -1E+20 0.76  0.15  1.0  0.01   28.88e6  FALSE  1.0  12  TRUE  TRUE  TRUE
  0.0 TRUE  1.50 -1E+20 0.76  0.46  1.0  0.01   28.88e6  FALSE  1.0  12  TRUE  TRUE  TRUE
  0.0 TRUE  1.50 -1E+20 0.76  0.25  1.0  0.01   28.88e6  FALSE  1.0  12  TRUE  TRUE  TRUE
  0.0 TRUE  1.50 -1E+20 0.76  0.45  1.0  0.01   19.62e6  FALSE  1.0  12  TRUE  TRUE  TRUE
  0.0 TRUE  1.50 -1E+20 0.76  0.24  1.0  0.01   19.62e6  FALSE  1.0  12  TRUE  TRUE  TRUE
  0.0 TRUE  1.50 -1E+20 0.76  0.74  1.0  0.01   19.62e6  FALSE  1.0  12  TRUE  TRUE  TRUE
  0.0 TRUE  1.50 -1E+20 0.76  0.40  1.0  0.01   19.62e6  FALSE  1.0  12  TRUE  TRUE  TRUE

  0.0 TRUE  1E+20 1.60 0.16  2.00   1.0  0.01   11.8e6  TRUE   11.40 9  FALSE  FALSE  FALSE
  0.0 TRUE  1E+20 1.60 0.20  2.00   1.0  0.01   15.0e6  TRUE   10.80 9  FALSE  FALSE  FALSE

 &OPTIMA
    OPT_METH = 7,  OPT_ITER = 300, OPT_TOL = 1.d-5,
    OPT_RESTART = FALSE, GRADIENT = 1, CDF = TRUE, FD_ETA  = 1.d-6,
    COEF_FRZ = FALSE, IFRZ_WHAT = 3, WFACTOR = 0.1, BSTEP = 0.1,
    AUTO_RESTART = FALSE, NUM_RESTARTS = 5,GRID_HIS = TRUE,
    SOL_HIS = FALSE, SC_METHOD = 2, USE_QUAD_PENALTY_METH = FALSE,

    JMSTART = 1, JMEND = 289, JMINC = 1, KMSTART = 2, KMEND = 65,
    KMINC = 1, RHO = 31,

    INORD = 2, IREORD = 2,
    ILU_METH = 2, LFIL = 6, PDC = 3.0,
    IM_GMRES = 85, EPS_GMRES = 1.d-8, ITER_GMRES = 500,

    NTCON=2, WFD=0.0, WTC=50.0,
    CTX     =0.95,0.99,
    CTY_TAR =0.010000075,0.002,

    WAC=0.0, AREAFAC=1.0

    NRTCON = 1, crtxl = 0.10d0, crtxt = 0.90d0, crtxn = 15,
    crthtar = 0.11844981
 &END
 &CYCLONE
    JMAX=289, KMAX=65, JTAIL1=33, JTAIL2=257,

    TRANSLO=0.01, TRANSUP=0.01,
```

```
   CLINPUT= 0.17, CLTOL=1.0d-11,
   RELAXCL=3.0,   ICLFREQ=50,   ICLSTRT=100,

   RESTART=FALSE, JACDT=1, IREAD=2, BCAIRF=TRUE, CIRCUL=FALSE,
   IORD=2, INTEG=2, CMESH=FALSE,

   IDMODEL=1,
   DIS2X   = 0.0,  DIS4X = 0.02,  DIS2Y = 0.0,  DIS4Y = 0.02,
   VLXI    = 0.25, VNXI  = 0.25,  VLETA = 0.25, VNETA = 0.25,
   LIMITER = 1,    EPZ   = 1.d-3, EPV   = 5.d0,

   PREC = 0, PRXI = 0.0, PRPHI = 1.0,

   TURBULNT = TRUE, ITMODEL = 2,    ISPBC = 1,     VISCEIG  = 1.d0,
   VISCOUS  = TRUE, VISETA  = TRUE, VISXI = FALSE, VISCROSS = FALSE,

   NCP = 1000, NQ = 1000,

   SNGVALTE   = FALSE, GRDSEQ_REST = FALSE, SV_GRDSEQ = FALSE,
   WRITERESID = FALSE, TIMING      = FALSE, WRITETURB = FASLE,
   FLBUD      = FALSE, PCHORD      = 0.32,  SKNFRC    = TRUE
&END
&PROBE
   NK_ITS = 100,   NK_ILU   = 2,  NK_LFIL  = 2, NK_PFRZ  = 1,
   NK_PDC = 6.d0, NK_IMGMR = 40, NK_ITGMR = 40
&END
&EXTRA
   grid_file_prefix = 'grid-new',
   output_file_prefix = 'test',
   restart_file_prefix = 'rest01'
&END
&GRAPH
   graphout = false, graph_mode = 1, interval = 0,
   num_graph= 0,
   graph_pt= 0
&END
1.E-6  | AF Convergence criteria: AF_MINR
5.E-13                          | Convergence criteria: MIN_RES
1.E-8                           | Min. res. in turb. mod. : SPMIN_RES
ISEQUAL
     1
   JMXI    KMXI    IENDS    DTISEQ   DTMIS   DTOW
   289     65      20000      5.0     0.0    1.d1
```